LBL-1413

c.2

THE VISCOSITY OF CESIUM METAL TO ITS CRITICAL TEMPERATURE

Han-Chung Tsai

(PhD Thesis)

July 1973

Prepared for the U. S. Atomic Energy Commission
under Contract W-7405-ENG-48

LAWRENCE BERKELEY LABORATORY
UNIVERSITY OF CALIFORNIA
BERKELEY

TWO-WEEK LOAN COPY

This is a Library Circulating Copy which may be borrowed for two weeks. For a personal retention copy, call Tech. Info. Division, Ext. 5545

LBL-1413
c.2

DISCLAIMER

This document was prepared as an account of work sponsored by the United States Government. While this document is believed to contain correct information, neither the United States Government nor any agency thereof, nor the Regents of the University of California, nor any of their employees, makes any warranty, express or implied, or assumes any legal responsibility for the accuracy, completeness, or usefulness of any information, apparatus, product, or process disclosed, or represents that its use would not infringe privately owned rights. Reference herein to any specific commercial product, process, or service by its trade name, trademark, manufacturer, or otherwise, does not necessarily constitute or imply its endorsement, recommendation, or favoring by the United States Government or any agency thereof, or the Regents of the University of California. The views and opinions of authors expressed herein do not necessarily state or reflect those of the United States Government or any agency thereof or the Regents of the University of California.

The Viscosity of Cesium Metal to Its Critical Temperature

Contents

Nomenclature iv

Abstract ix

I. Introduction 1

II. Theory of the Oscillating Cup Viscometer 8

A. Liquid Phase Only 8

B. Two Phases 14

III. Experimental Apparatus 23

A. General Description 23

B. Vacuum System 26

C. Pendulum Motion Recording System 26

D. Torsion Wire Preparation 33

E. Tungsten Crucible Design 33

IV. Experimental Procedure 38

A. Sample Preparation 38

B. Moment of Inertia Measurement 40

C. Viscosity Measurement 41

V. Results 42

VI. Discussion 49

A. Law of Rectilinear Diameters: The Critical Viscosity of Cesium 49

B. Andrade's Theory of Liquid Viscosity 51

C. Theory of Corresponding States: Viscosities of Sodium and Potassium 52

Acknowledgement 59

References 60

NOMENCLATURE

A	Constant defined in Eq. (40).
a	Inside diameter of the crucible
A_n	Constants defined in Eq. (28)
b	$\sqrt{\alpha/\nu}$
B_n	Constants defined in Eq. (28)
E_o	amplitude of the energy barrier
$\underline{f}$	Spring constant of the torsion fibre
$F_{r,\phi,\theta}$	Body forces of the fluid in the r, ϕ, θ directions
G	Damping torque
g	gravitational constant
H	height of the crucible
h	height of the liquid
I	Moment of inertia of the oscillating system without the sample
I_o	Moment of inertia of the oscillating system including the sample
j_n	positive roots of $J_1(Z) = 0$
k	Boltzmann's constant
k_n	j_n/a
L	Damping coefficient of the pendulum motion
ℓn	Parameters defined in Eqs. (30a) and (30b).
M	Molecular weight of the liquid metal
m	$\sqrt{-\alpha/\nu}$
n	Molecular density of the liquid metal
N_o	Avogadro's number
P	Pressure in the fluid
P_c	Critical pressure

R	Gas constant
r	r-coordinate
T	Period of pendulum motion without the inertia rod
t	Time interval between each two triggerings of the photocell
T^*	Reduced temperature
T_c	Critical temperature
T_m	Melting temperature of the liquid metal
T_1	Period of pendulum motion with the inertia rod
V	Specific volume
V^*	Reduced volume
$v_{r,\phi,z}$	Linear velocities of the fluid in the r, ϕ, z directions
x	$\frac{\pi t/\tau}{\tan(\pi t/\tau)}$
Z	H-z
z	z-coordinate
α	$-\beta+i\gamma$
β	Decay constant of the pendulum motion
γ	$2\pi/\tau$
ε	Depth of the potential well between molecules
η	Dynamic viscosity
$\bar{\eta}$	Mean viscosity of the liquid and the saturated vapor
η^*	Reduced viscosity
η_c	Critical viscosity
η_c^*	Reduced critical viscosity
θ	Angular displacement of the oscillating motion
ν	Kinematic viscosity; η/ρ

ρ	Density of the fluid
ρ_c	Critical density
σ	Collision diameter of the intermolecular potential function
τ	Period of the oscillating motion
Φ	Spatial component of the angular velocity of the fluid
ϕ	ϕ-coordinate
Φ_o	Angular velocity of the pendulum at time = 0
ψ	Angular velocity of the fluid

The Viscosity of Cesium Metal to Its Critical Temperature

Han-Chung Tsai

Inorganic Materials Research Division, Lawrence Berkeley Laboratory, and Department of Nuclear Engineering, College of Engineering, of the University of California, Berkeley, California 94720

ABSTRACT

Cesium metal viscosity has been measured up to 1600°C by oscillating cup techniques. Viscous drag due to the saturated vapor phase has been taken into account in the data analysis. The measured result can be represented by the equations

$$\ln \eta \text{ (mP)} = -0.187 + \frac{6.34\times10^2}{T}, \quad 410°K \leq T \leq 1100°K$$

$$\ln \eta \text{ (mP)} = -2.55 + \frac{6.01\times10^3}{T} - \frac{3.10\times10^6}{T^2}, \quad 1100°K < T < 1900°K.$$

The critical viscosity of cesium determined from the law of rectilinear diameters is 0.57 ± .04 millipoise.

Viscosities of sodium and potassium were also estimated from the cesium data by the law of corresponding states.

I. INTRODUCTION

Alkali metals are of interest as high temperature coolants and working fluids in numerous nuclear and space applications. Viscosity is among one of the transport properties which are required for rational design of systems involving alkali metals for such applications.

In determining high temperature fluid viscosity, there are four commonly used techniques, namely, capillary method, falling sphere method, rotational viscometer and oscillating cup viscometer.[1]

In the capillary method, the viscosity is determined by measuring the rate of fluid flow through the capillary tube as a function of applied pressure or liquid heads. Although its theory is simple and exact, the method suffers two main disadvantages: 1) the accuracy of the measured result relies critically on the accuracy of the capillary diameter, 2) an open flow system has to be maintained over a uniform temperature zone. This method, however, is popular in alkali metal vapor and molten salt viscosity determinations.[2-4]

In the falling sphere method, a round ball with a greater specific gravity than the liquid is dropped into the liquid under investigation and the asymptotic velocity of the ball then determines the liquid viscosity. The main difficulties associated with this technique are to keep a large column of high temperature/high pressure fluid and to measure accurately the ball speed.[5]

The rotational viscometer is a cylindrical body immersed in a concentric

cylindrical bath filled with the fluid whose viscosity is to be determined. Relative angular velocity between the body and the bath is maintained constant and the torque required for this relative motion is measured and used to determine the fluid viscosity. The difficulty of measuring the torque makes this method relatively inaccurate. The rotational viscometer is, therefore, used mostly for high viscosity materials like glasses and slags.[6]

The oscillating cup viscometer is a cylindrical crucible containing the fluid and suspended by a piece of wire. Torsional oscillation about the vertical axis, initiated by a twist of the wire, is damped by the viscous drag of the fluid inside. The degree of damping is related to the fluid viscosity. The theory of oscillating cup viscometer has been discussed in detail by Roscoe[7] and Thresh[8].

One of the advantages of this method is that the fluid is contained in a sealed crucible so that the problems associated with vaporization and chemical reaction with the surrounding atmosphere are avoided. Another merit is that the hot zone can be relatively small and the temperature uniformity can be more easily achieved. Also, the decay constant and the oscillation period of the motion can be measured with high degree of accuracy. Because of these advantages, oscillating cup technique is adopted for the present study of cesium metal viscosity.

The crucible used in the oscillating cup technique has essentially a constant volume and because of the thermal expansion of the sample fluid, complete filling of the crucible with the liquid is not possible if one sample is to be studied over a range of temperatures. As a result, there is always a space in the crucible on top of the liquid

phase which is occupied by the saturated vapor. For low temperature experiments, the viscous drag due to the vapor phase is small and may be neglected. This condition is not valid at high temperatures when the liquid metal has high vapor pressure. In addition to the high vapor pressure, the temperature dependences of the liquid and vapor viscosities accentuates this effect. The liquid viscosity decrease with temperature owing to the positive activation energy of this transport property,[9] but the vapor viscosity increases with temperature due to the increased translational momentum transfer.[10] The liquid and vapor viscosities approach each other at high temperature and ultimately become equal at the critical point.[11]

The precision of the decay constant measurement in the oscillating cup technique is proportional to the sample viscosity and inversely proportional to the system moment of inertia. In the high temperature measurements, thick-wall crucibles are required to contain the high pressure vapor. The bulky crucibles have a large moment of inertia. In addition, the viscosity of liquid is low at high temperature. Indeed these phenomena might be the ultimate limitations on the use of the oscillating cup technique for measuring the viscosity of substances at temperatures where the vapor pressure is high.

Among the alkali metals, cesium was chosen for study for the following reasons:

(a) it has the lowest critical temperature and pressure,[12]

(b) its critical constants have all been measured and are fairly well established,[12] and

c) it is compatible with tungsten, the crucible material, up to the critical point.[13]

The critical constants of cesium reported by several investigators are shown in Table I. In our research only the critical temperature is of immediate concern. A mean temperature of 1760°C from the three values shown in Table I is used.

Table I. Critical Constants of Cesium

Investigator	T_c (°K)	ρ_c (gm-cm^{-3})	P_c (atm)
Dillon et al.[14]	2057 ± 40	0.428 ± .012	-
Renkert and Franck[15]	1993 ± 30	-	104 ± 10
Bonilla et al.[16]	2050	0.445	117
Mean value	2033	0.436	113

The variation of cesium vapor pressure with temperature has been measured by Renkert and Franck,[15] and Stone et al.,[17] and is shown in Fig. 1.

Density data for both liquid and saturated vapor of cesium are obtained from Ref. 18. The densities versus temperature plot is shown in Fig. 2. Change of the densities of the two phases with temperature is similar to that of the viscosities, i.e., the liquid and the vapor properties approach each other and become equal at the critical temperature.

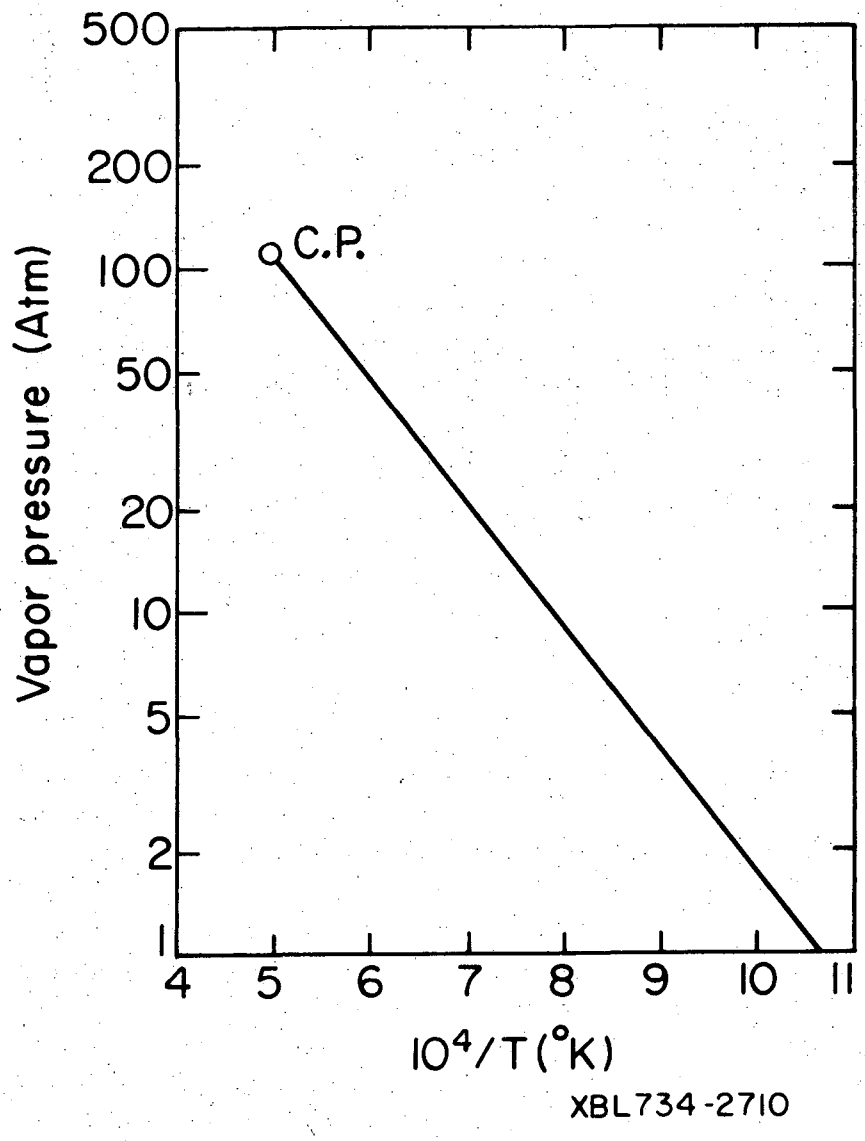

Fig. 1. Vapor pressure of cesium.

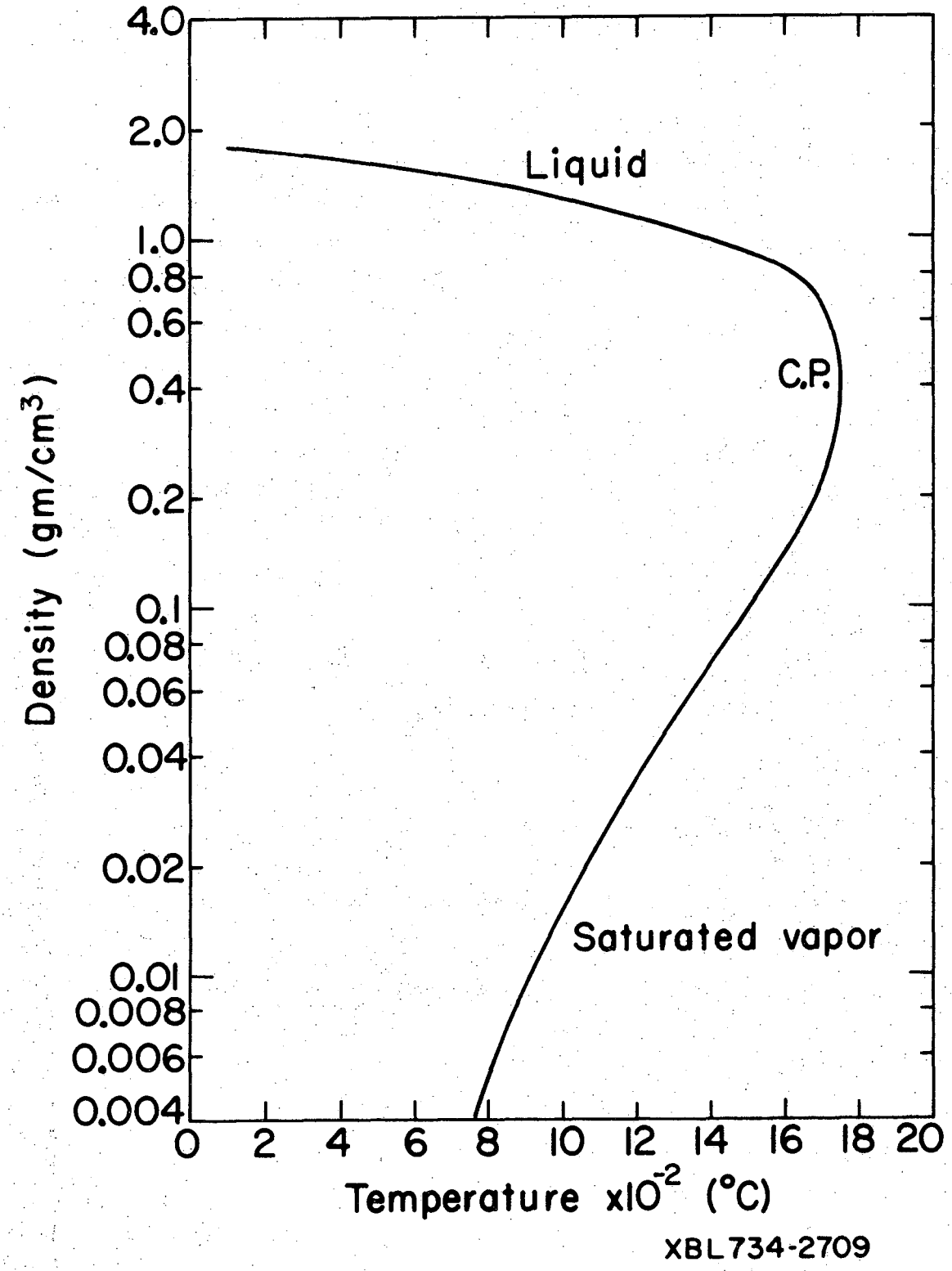

Fig. 2. Densities of the liquid and the saturated vapor of cesium.

Since the viscous drag due to the vapor phase becomes significant at high temperatures, a two-phase mathematical solution to the fluid mechanics of the oscillating cup viscometer which allows the vapor drag to be taken into account was developed and employed in this cesium viscosity research.

Cesium viscosity was measured up to 1600°C, which is 160°C below the reported critical temperature. Similarity of the properties between the alkali metals indicates that the law of corresponding states of the liquid viscosities should apply to this class of substances. The measured cesium viscosity was used to construct the universal viscosity-temperature function in the way suggested by Chapman[19] and Pasternak.[20] This correlation is of value since direct measurement of the viscosities of the other alkali metals is more difficult due to the high critical temperatures and pressures.

II. THEORY OF THE OSCILLATING CUP VISCOMETER

The oscillating cup viscometer is essentially a pendulum system composed of a sealed right circular crucible, which contains the fluid under investigation, suspended by a piece of torsion fibre. The drag of the viscous fluid inside the crucible causes damping of the oscillatory motion and the measurable damping effect is a function of the viscosity of the fluid. At relatively low temperature, only the liquid phase exerts the drag on the pendulum. The theory for this case has been worked out by Roscoe[7] and Hopkins and Toye.[21] At higher temperatures, especially as the critical point is approached, the drag due to the saturated vapor phase above the liquid is also appreciable and has to be taken into account. This extension is presented here.

A. Liquid Phase Only

The Navier-Stokes equations for the liquid are to be solved along with the appropriate boundary conditions. Assuming the fluid is Newtonian and incompressible, the equations of motion are

$$\rho\left(\frac{\partial v_r}{\partial t} + v_r \frac{\partial v_r}{\partial r} + \frac{v_\phi}{r}\frac{\partial v_r}{\partial \phi} - \frac{v_\phi^{\,2}}{r} + v_z \frac{\partial v_r}{\partial z}\right)$$

$$= F_r - \frac{\partial P}{\partial r} + \eta\left(\frac{\partial^2 v_r}{\partial r^2} + \frac{1}{r}\frac{\partial v_r}{\partial r} - \frac{v_r}{r^2} + \frac{1}{r^2}\frac{\partial^2 v_r}{\partial \phi^2} - \frac{2}{r^2}\frac{\partial v_\phi}{\partial \phi} + \frac{\partial^2 v_r}{\partial z^2}\right) \qquad \text{(1a)}$$

$$\rho\left(\frac{\partial v_\phi}{\partial t} + v_r \frac{\partial v_\phi}{\partial r} + \frac{v_\phi}{r}\frac{\partial v_\phi}{\partial \phi} + \frac{v_r v_\phi}{r} + v_z \frac{\partial v_\phi}{\partial z}\right)$$

$$= F_\phi - \frac{1}{r}\frac{\partial P}{\partial \phi} + \eta\left(\frac{\partial^2 v_\phi}{\partial r^2} + \frac{1}{r}\frac{\partial v_\phi}{\partial r} - \frac{v_\phi}{r^2} + \frac{1}{r^2}\frac{\partial^2 v_\phi}{\partial \phi^2} + \frac{2}{r^2}\frac{\partial v_r}{\partial \phi} + \frac{\partial^2 v_\phi}{\partial z^2}\right) \quad (1b)$$

$$\rho\left(\frac{\partial v_z}{\partial t} + v_r \frac{\partial v_z}{\partial r} + \frac{v_\phi}{r}\frac{\partial v_z}{\partial \phi} + v_z \frac{\partial v_z}{\partial z}\right)$$

$$= F_z - \frac{\partial P}{\partial z} + \eta\left(\frac{\partial^2 v_z}{\partial r^2} + \frac{1}{r}\frac{\partial v_z}{\partial r} + \frac{1}{r^2}\frac{\partial^2 v_z}{\partial \phi^2} + \frac{\partial^2 v_z}{\partial z^2}\right) \quad (1c)$$

where v_r, v_ϕ, v_z are the velocity components in the r, ϕ, z directions,

F_r, F_ϕ, F_z are the components of the body force in the r, ϕ, z directions,

ρ is the density of the liquid,

P is the pressure,

η is the dynamic viscosity of the liquid.

Assuming that

1. v_r and v_z are zero,
2. v_ϕ is independent of ϕ,
3. pressure P is also independent of ϕ,
4. the only body force on the liquid is its own weight,

then the equations (1a), (1b), (1c) can be reduced to

$$\rho \frac{v_\phi^2}{r} = \frac{\partial P}{\partial r} \quad (2a)$$

$$\rho \frac{\partial v_\phi}{\partial t} = \eta\left(\frac{\partial^2 v_\phi}{\partial r^2} + \frac{1}{r}\frac{\partial v_\phi}{\partial r} - \frac{v_\phi}{r^2} + \frac{\partial^2 v_\phi}{\partial z^2}\right) \tag{2b}$$

$$F_z = \frac{\partial P}{\partial z} = -g \, . \tag{2c}$$

In terms of angular velocity ($\psi = \frac{v_\phi}{r}$) and kinematic viscosity ($\nu = \frac{\eta}{\rho}$), Eq.(2b) can be rewritten as

$$\frac{1}{\nu}\frac{\partial \psi}{\partial t} = \frac{\partial^2 \psi}{\partial r^2} + \frac{3}{r}\frac{\partial \psi}{\partial r} + \frac{\partial^2 \psi}{\partial z^2} \, . \tag{3}$$

If the system has settled down such that at any point the liquid and the containing vessel have the same period and decay constant, we may separate the time and spatial components of the angular velocity as

$$\psi(r,z,t) = \Phi(r,z)\, e^{\alpha t} \tag{4}$$

where

$$\alpha = -\beta + i\gamma \, . \tag{5}$$

β is the decay constant and γ is the angular velocity of the pendulum motion. The latter is related to the period of oscillation, τ, by

$$\gamma = \frac{2\pi}{\tau} \, . \tag{6}$$

Substituting Eq.(4) into Eq.(3), we get

$$\frac{\alpha}{\nu}\Phi = \frac{\partial^2 \Phi}{\partial r^2} + \frac{3}{r}\frac{\partial \Phi}{\partial r} + \frac{\partial^2 \Phi}{\partial z^2} \tag{7}$$

which is the final version of the equation to be solved for the velocity profile of the liquid inside the vessel.

The boundary conditions are

(I) $\Phi = \Phi_o$ at $r = a$ and $z = 0$ (8a)

(II) $\frac{\partial \Phi}{\partial z} = 0$ at $z = h$ (8b)

where Φ_o is the angular velocity of the crucible body when passing the equilibrium position, a is the inside radius of the crucible and h is the height of the liquid (Fig. 3). The second boundary condition is equivalent to no shear force from the top of the liquid which is assumed to be vacuum.

The equation of the motion of the oscillating system is

$$I \frac{d^2\Theta}{dt^2} + L \frac{d\Theta}{dt} + f\Theta = 0 \tag{9}$$

where

I = moment of inertia of the empty system,

L = damping coefficient due to the viscous drag,

f = spring constant of the torsion fibre,

θ = angular displacement of the oscillation motion.

The solution of Eq.(7) which satisfies the boundary condition is [21]

$$\Phi(r,z) = \frac{a\ \Phi_o\ J_1(ibr)}{r\ \ J_2(iba)} - \frac{2\Phi_o a}{r} \sum_{n=1}^{\infty} \frac{J_1(j_n r/a) b^2 a^2 \cosh\left[(j_n{}^2+b^2a^2)^{1/2}\ \frac{z-h}{a}\right]}{J_2(j_n) j_n (j_n{}^2+b^2a^2)^{1/2} \cosh\left[(j_n^2+b^2a^2)^{1/2} \frac{h}{a}\right]} \tag{10}$$

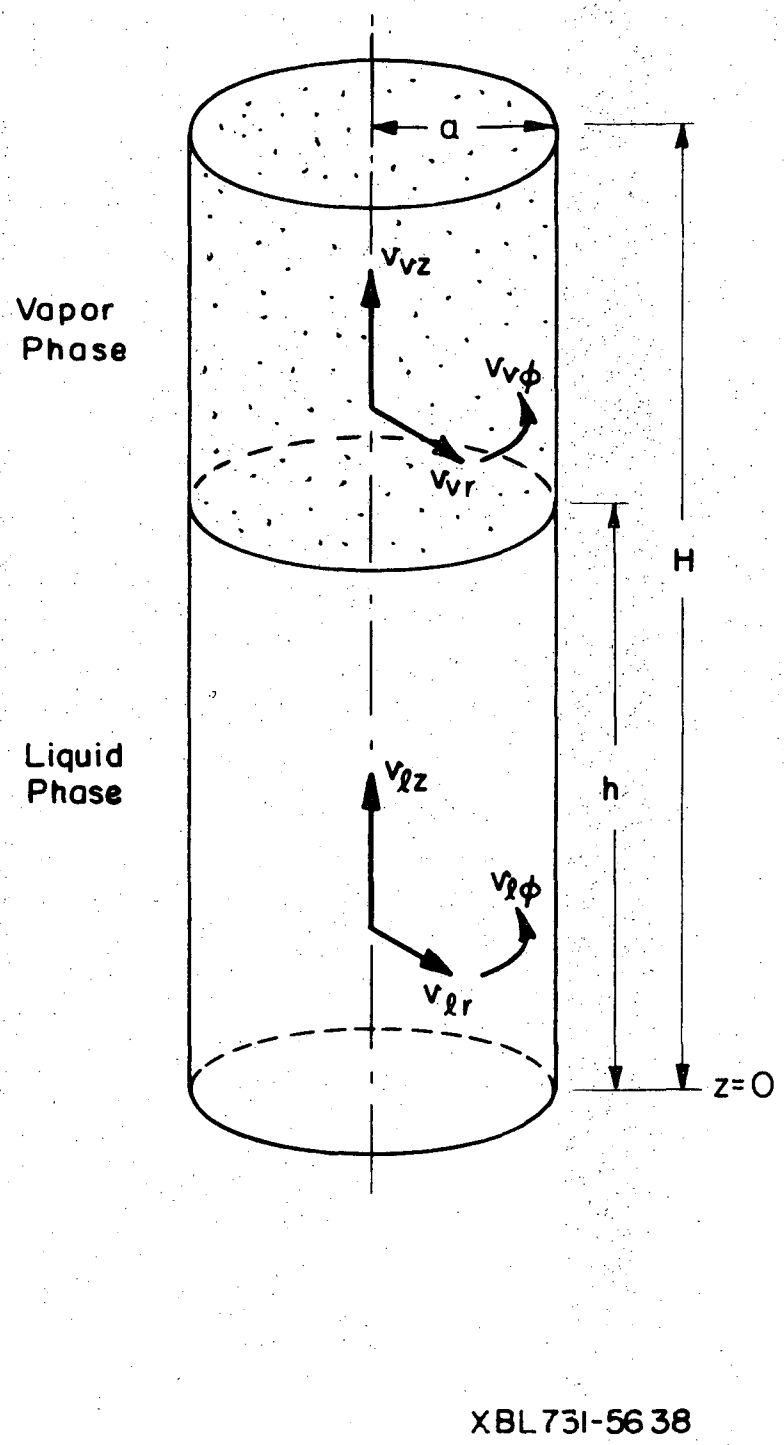

Fig. 3. Fluids in the containing vessel.

where $b^2 = \alpha/\nu$ and j_n's are the positive roots of $J_1(z) = 0$ in ascending order of magnitude. The damping torque G due to the viscous drag of the liquid on the inside wall of the crucible is then

$$G = 2\pi\eta e^{\alpha t}\left[a^3 \int_0^h \left(\frac{\partial\Phi}{\partial r}\right)_{r=a} dz - \int_0^a \left(\frac{\partial\Phi}{\partial z}\right)_{z=0} r^3\, dr \right] \tag{11}$$

The damping coefficient L, which is related to the torque G by

$$G = L\frac{d\theta}{dt} \tag{12}$$

can then be determined. Since the pendulum motion is damped sinusoidally

$$\frac{d\Theta}{dt} = \Phi_o\, e^{\alpha t} \quad . \tag{13}$$

Combining Eqs.(11), (12), (13) and solving for L, we get

$$L = 2\pi\eta\left[a^3 \int_0^h \left(\frac{\partial(\Phi/\Phi_o)}{\partial r}\right)_{r=a} dz - \int_0^a \left(\frac{\partial(\Phi/\Phi_o)}{\partial z}\right)_{z=0} r^3\, dr \right] . \tag{14}$$

To calculate L, it is convenient to follow Roscoe's process of simplifying Eq.(14) into a rapidly converging series:[7]

$$L = 2\pi\eta\left\{ ba^3h\left[1 - \frac{3}{2(ba)} + \frac{3}{8(ba)^2} + \frac{3}{8(ba)^3} + \frac{63}{128(ba)^4} + \cdots\right] + 2ba^4\left[\frac{1}{8} - \frac{2}{\pi(ba)} + \frac{9}{8(ba)^2} - \frac{1}{\pi(ba)^3} - \frac{45}{128(ba)^4} + \cdots\right]\right\} . \tag{15}$$

Recall Eq.(9), which by writing $\Theta = \Theta_o\, e^{\alpha t}$, becomes

$$I\alpha^2 + L\alpha + f = 0 \ . \tag{16}$$

Since α and L are both complex, Eq.(16) can be separated into real and imaginary parts:

$$I(\beta^2 - \gamma^2) + \beta \mathrm{Re}(L) - \gamma \ \mathrm{Im}(L) + f = 0 \tag{17}$$

$$-2I\beta\gamma - \beta \mathrm{Im}(L) + \gamma \ \mathrm{Re}(L) = 0 \ . \tag{18}$$

Eq.(18) is preferred over Eq.(17) because it does not contain the torsion wire spring constant f. The viscosity η can now be determined by solving Eq.(18) and Eq.(15) simultaneously since all the other quantities are measurable or known. Application of the liquid phase solution is illustrated in Ref. 22.

B. Two Phases

When the temperature is far below the critical temperature, the viscous drag due to the vapor phase in an oscillating cup viscometer is negligible compared to that of the liquid. As the critical point is approached, however, the dynamic viscosity of the saturated vapor becomes comparable to that of the liquid and finally becomes equal to the latter at the critical point. When a viscometer only partially filled with liquid is operated at high temperature, it is necessary to solve the equation of motion in both phases.

After the transient part of the motion has been passed, we can assume that

$$v_{\ell r} = v_{vr} = 0$$

$$v_{\ell z} = v_{vz} = 0$$

$$\frac{\partial v_{\ell\phi}}{\partial\phi} = \frac{\partial v_{v\phi}}{\partial\phi} = 0$$

where v's are the components of the linear velocities of the liquid and vapor phases as shown in Fig. 3. The subscripts ℓ and v refer to liquid and vapor phases, respectively.

As in the single phase case, the Navier-Stokes equations can be reduced to

$$\rho_\ell \frac{v_{\ell\phi}^{\ 2}}{r} = \frac{\partial P_\ell}{\partial r} \tag{19a}$$

$$\rho_\ell \frac{\partial v_{\ell\phi}}{\partial t} = \eta_\ell \left(\frac{\partial^2 v_{\ell\phi}}{\partial r^2} + \frac{1}{r}\frac{\partial v_{\ell\phi}}{\partial r} - \frac{v_{\ell\phi}}{r^2} + \frac{\partial^2 v_{\ell\phi}}{\partial z^2} \right) \tag{19b}$$

$$F_{\ell z} = -g = \frac{\partial P_\ell}{\partial z} \tag{19c}$$

for the liquid phase and similarly

$$\rho_v \frac{v_{v\phi}^{\ 2}}{r} = \frac{\partial P_v}{\partial r} \tag{20a}$$

$$\rho_v \frac{\partial v_{v\phi}}{\partial t} = \eta_v \left(\frac{\partial^2 v_{v\phi}}{\partial r^2} + \frac{1}{r}\frac{\partial v_{v\phi}}{\partial r} - \frac{v_{v\phi}}{r^2} + \frac{\partial^2 v_{\ell\phi}}{\partial z^2} \right) \tag{20b}$$

$$F_{vz} = -g = \frac{\partial P_v}{\partial z} \tag{20c}$$

for the vapor phase, where

ρ_ℓ = density of the liquid,

ρ_v = density of the saturated vapor,

η_ℓ = dynamic viscosity of the liquid,

η_v = dynamic viscosity of the saturated vapor,

$F_{\ell z}$ = body force in the liquid,

F_{vz} = body force in the vapor,

P_ℓ = pressure in the liquid,

P_v = pressure in the vapor .

Again, we can express Eqs. (19b), (20b) in terms of kinematic viscosities

$$\nu_\ell = \frac{\eta_\ell}{\rho_\ell} \tag{21a}$$

$$\nu_v = \frac{\eta_v}{\rho_v} \tag{21b}$$

and angular velocities

$$\psi_\ell = \frac{v_{\ell\phi}}{r} \tag{22a}$$

$$\psi_v = \frac{v_{v\phi}}{r} \tag{22b}$$

as

$$\frac{1}{\nu_\ell}\frac{\partial\psi_\ell}{\partial t} = \frac{\partial^2\psi_\ell}{\partial r^2} + \frac{3}{r}\frac{\partial\psi_\ell}{\partial r} + \frac{\partial^2\psi_\ell}{\partial z^2} \tag{23a}$$

and

$$\frac{1}{\nu_v}\frac{\partial\psi_v}{\partial t} = \frac{\partial^2\psi_v}{\partial r^2} + \frac{3}{r}\frac{\partial\psi_v}{\partial r} + \frac{\partial^2\psi_v}{\partial z^2} \quad . \tag{23b}$$

Further assume that the system has settled down such that at any point the fluid and the containing vessel have the same period and decay constant, so we can again write

$$\psi_\ell(r,z,t) = \Phi_\ell(r,z)\, e^{\alpha t} \tag{24a}$$

$$\psi_v(r,z,t) = \Phi_v(r,z)\, e^{\alpha t} \tag{24b}$$

where $\alpha = -\beta + i\gamma$ with γ defined as $2\pi/\tau$; τ is the period of the oscillation and β the decay constant of the system. Notice that α is the same for both phases because the system has only one period and one decay constant. Substituting Eqs. (24a), (24b) into Eqs. (23a) and (23b), we get for the liquid phase

$$\frac{\alpha}{\nu_\ell}\Phi_\ell = \frac{\partial^2\Phi_\ell}{\partial r^2} + \frac{3}{r}\frac{\partial\Phi_\ell}{\partial r} + \frac{\partial^2\Phi_\ell}{\partial z^2} \tag{25a}$$

and for the vapor phase

$$\frac{\alpha}{\nu_v}\Phi_v = \frac{\partial^2\Phi_v}{\partial r^2} + \frac{3}{r}\frac{\partial\Phi_v}{\partial r} + \frac{\partial^2\Phi_v}{\partial z^2} \quad . \tag{25b}$$

Equations (25a) and (25b) are the two equations to be solved for the velocity profiles of the fluids inside the containing vessel.

The boundary conditions are

$$\text{(I)} \quad \Phi_\ell = \Phi_o \quad \text{at } r = a \text{ and } z = 0, \tag{27a}$$

$$\text{(II)} \quad \Phi_v = \Phi_o \quad \text{at } r = a \text{ and } z = H, \tag{27b}$$

$$\text{(III)} \quad \Phi_\ell = \Phi_v \quad \text{at } z = h\ , \tag{27c}$$

$$\text{(IV)} \quad \eta_\ell \frac{\partial\phi_\ell}{\partial z} = -\eta_v \frac{\partial\Phi_v}{\partial z} \quad \text{at } z = h\ . \tag{27d}$$

Φ_o is the angular velocity of the crucible when it is passing the equilibrium position, in other words, $\Phi_o\, e^{\alpha t}$ is the angular velocity of the crucible. Condition (III) assumes no slip at the interface and condition (IV) represents the continuity of shear stress at the interface.

A series expression

$$\Phi_\ell = \sum_{n=1}^{\infty} [A_n^\ell \sinh \ell_n^\ell z + B_n^\ell \cosh \ell_n^\ell (h-z)] \frac{J_1(k_n r)}{r} + \frac{a\Phi_o}{r} \frac{J_1(m_\ell r)}{J_1(m_\ell a)} \tag{28}$$

is assumed for the solution of Eq.(25a), where J_1 is the Bessel function of order one and $J_1(k_n a) = 0$, A_n^ℓ, B_n^ℓ are constants to be determined and

$$m_\ell^{\,2} = -\frac{\alpha}{\nu_\ell} \tag{29a}$$

$$(\ell_n^\ell)^2 = k_n^{\,2} - m_\ell^{\,2} \quad . \tag{30a}$$

The subscript and superscript ℓ refer to liquid phase.

It is evident that Eq.(28) satisfies the first part of the boundary condition (I), namely, $\Phi_\ell = \Phi_o$ at $r = a$. The condition $\Phi_\ell = \Phi_o$ at $z = 0$ requires*

---

* At $z = 0$, $\sinh \ell_n^\ell z = 0$ and $\cosh \ell_n^\ell (h-z) = \cosh \ell_n^\ell h$ and the following equality can be proved:

$$\sum_{n=1}^{\infty} \frac{2m_\ell^{\,2}\, \Phi_o}{J_2(k_n a) k_n (\ell_n^\ell)^2} \frac{J_1(k_n r)}{r} + \frac{a\Phi_o}{r} \frac{J_1(m_\ell r)}{J_1(m_\ell a)} = \Phi_o \quad .$$

$$B_n^{\ell} = \frac{2m_{\ell}^{2}\,\Phi_o}{J_2(k_n a)k_n(\ell_n^{\ell})^2\cosh(\ell_n^{\ell}h)} \quad . \tag{31}$$

Substituting Eq.(31) into Eq.(28) yields

$$\Phi_{\ell} = \sum_{n=1}^{\infty}\left\{A_n^{\ell}\sinh(\ell_n^{\ell}z) + \frac{2m_{\ell}^{2}\,\Phi_o}{J_2(k_n a)k_n(\ell_n^{\ell})^2\cosh(\ell_n^{\ell}h)}\cosh[\ell_n^{\ell}(h-z)]\right\}\frac{J_1(k_n r)}{r}$$

$$+\frac{a\Phi_o}{r}\,\frac{J_1(m_{\ell}r)}{J_1(m_{\ell}a)} \quad . \tag{32a}$$

Similarly the solution for the vapor phase can be expressed in the same form

$$\Phi_v = \sum_{n=1}^{\infty}\left\{A_n^{v}\sinh(\ell_n^{v}Z) + \frac{2m_v^{2}\Phi_o}{J_2(k_n a)k_n(\ell_n^{v})^2\cosh[\ell_n^{v}(H-h)]}\cosh[\ell_n^{v}(H-h-Z)]\right\}\frac{J_1(k_n r)}{r}$$

$$+\frac{a\Phi_o}{r}\,\frac{J_1(m_v r)}{J_1(m_v a)} \tag{32b}$$

where the axial coordinate in the vapor phase has been changed to $Z = H-z$.

Parallel to that of the liquid phase, m_v and ℓ_n^{v} in Eq.(32b) are defined as follows:

$$m_v^{2} = -\frac{\alpha}{\nu_v} \tag{29b}$$

$$(\ell_n^{v})^2 = k_n^{2} - m_v^{2} \quad . \tag{30b}$$

To determine A_n^ℓ's and A_n^v's, the other two boundary conditions have to be utilized. Equation (27d) permits A_n^v to be expressed in terms of A_n^ℓ:

$$A_n^v = \frac{\eta_\ell}{\eta_v}\frac{\ell_n^\ell}{\ell_n^v}\frac{\cosh(\ell_n^\ell h)}{\cosh(\ell_n^v(H-h)]}\ A_n^\ell \quad . \tag{33}$$

Substituting Eq.(33) into Eq.(32b) and combining Eq.(32a) with boundary condition III (Eq.(27c)); A_n^ℓ can be determined as:

$$\frac{A_n^\ell}{\Phi_o} = \left\{-\frac{2k_n^2}{(\ell_n^\ell)^2} + \frac{2k_n^2}{(\ell_n^v)^2} - \frac{2m_\ell^2}{(\ell_n^\ell)^2\cosh(\ell_n^\ell h)} + \frac{2m_v^2}{(\ell_n^v)^2\cosh[\ell_n^v(H-h)]}\right\} \Bigg/ J_2(k_n a)k_n \quad \sinh(\ell_n^\ell h) - \frac{\eta_\ell \ell_n^\ell}{\eta_v \ell_n^v}\cosh(\ell_n^\ell h)\tanh[\ell_n^v(H-h)] \quad . \tag{34}$$

A_n^v can thus be determined from Eq.(33) and Eq.(34).

The ratios of the maximum fluid velocities to that of the crucible are

$$\frac{\Phi_\ell}{\Phi_o} = \frac{aJ_1(m_\ell r)}{rJ_1(m_\ell a)} + \sum_{n=1}^{\infty}\left\{\frac{A_n^\ell}{\Phi_o}\sinh(\ell_n^\ell z) + \frac{2m_\ell^2}{J_2(k_n a)k_n(\ell_n^\ell)^2\cosh(\ell_n^\ell h)}\cosh[\ell_n^\ell(h-z)]\right\}\cdot \frac{J_1(k_n r)}{r} \tag{35a}$$

$$\frac{\Phi_v}{\Phi_o} = \frac{aJ_1(m_v r)}{aJ_1(m_v a)} + \sum_{n=1}^{\infty}\left\{\frac{A_n^v}{\Phi_o}\sinh(\ell_n^v Z) + \frac{2m_v^2}{J_2(k_n a)k_n(\ell_n^v)\ \cosh[\ell_n^v(H-h)]}\cdot \cosh[\ell_n^v(H-h-Z)]\right\}\frac{J_1(k_n r)}{r} \quad . \tag{35b}$$

The viscous drag G on the inside walls of the crucible due to the presence of liquid and saturated vapor is

$$G = \int_0^h 2\pi a^2 \eta_\ell \left(\frac{\partial a\Phi_\ell e^{\alpha t}}{\partial r}\right)_{r=a} dz$$

$$- \int_0^a \eta^\ell \left(\frac{\partial r\Phi_\ell e^{\alpha t}}{\partial z}\right)_{z=0} 2\pi r^2 dr$$

$$+ \int_0^{H-h} 2\pi a^2 \eta_v \left(\frac{\partial a\Phi_o e^{\alpha t}}{\partial r}\right)_{r=a} dZ$$

$$- \int_0^a \eta_v \left(\frac{\partial r\Phi_v e^{\alpha t}}{\partial Z}\right)_{Z=0} 2\pi r^2 dr \quad . \tag{36}$$

The damping coefficient L, as in the single phase case, can be expressed as

$$L = \frac{G}{\Phi_o} e^{\alpha t}$$

$$= 2\pi \left[\eta_\ell a^3 \int_0^h \left(\frac{\partial(\Phi_\ell/\Phi_o)}{\partial r}\right)_{r=a} dz - \eta_\ell \int_0^a \left(\frac{\partial(\Phi_\ell/\Phi_o)}{\partial z}\right)_{z=0} r^3 dr \right.$$

$$\left. + \eta_v a^3 \int_0^{H-h} \left(\frac{\partial(\Phi_v/\Phi_o)}{\partial r}\right)_{r=a} dZ - \eta_v \int_0^a \left(\frac{\partial(\Phi_v/\Phi_o)}{\partial Z}\right)_{Z=0} r^3 dr \right] . \tag{37}$$

To determine η_ℓ if η_v is known (or vice versa), Eqs.(37) and (18) must be solved simultaneously. It is also possible to determine both η_ℓ and η_v with two different measurements with different h values.

III. EXPERIMENTAL APPARATUS

A. General Description

The system is described with reference to the sectional diagram of Fig. 4.

The pendulum is made up of five parts, the crucible (D), in which the sample is held, the connecting rod (E), the thermal insulator (F), the external part of the pendulum (G) and the chuck (H). A photograph of the assembly is shown in Fig. 5. A polished surface on the external portion (G) is used to reflect the incident laser light (Z) by which the oscillating motion is monitored. This portion also has a horizontally drilled hole into which different inertia rods (I) can be inserted and fixed so that the moment of inertia of the pendulum can be adjusted. (See section B of experimental procedure.)

The pendulum system is suspended by a piece of torsion fibre (J) attached to a second chuck (K) which is fixed to a rotable holder (L). The holder, which rests on a supporting plate (M) is attached mechanically to a rotary feedthrough (N) by which oscillation of the pendulum is initiated through the vacuum wall.

The crucible is suspended in the hot zone of a Brew tungsten mesh furnace (A) of 1 3/4 inch diameter and 3 1/2 inch height. Layers of tungsten thermal shields arranged on the side, the top and the bottom reduce the radiation heat loss and also provide uniform temperature in the hot zone. Temperatures up to 1300°C are measured by a chromel-Alumel thermocouple located close to the crucible. An optical pyrometer

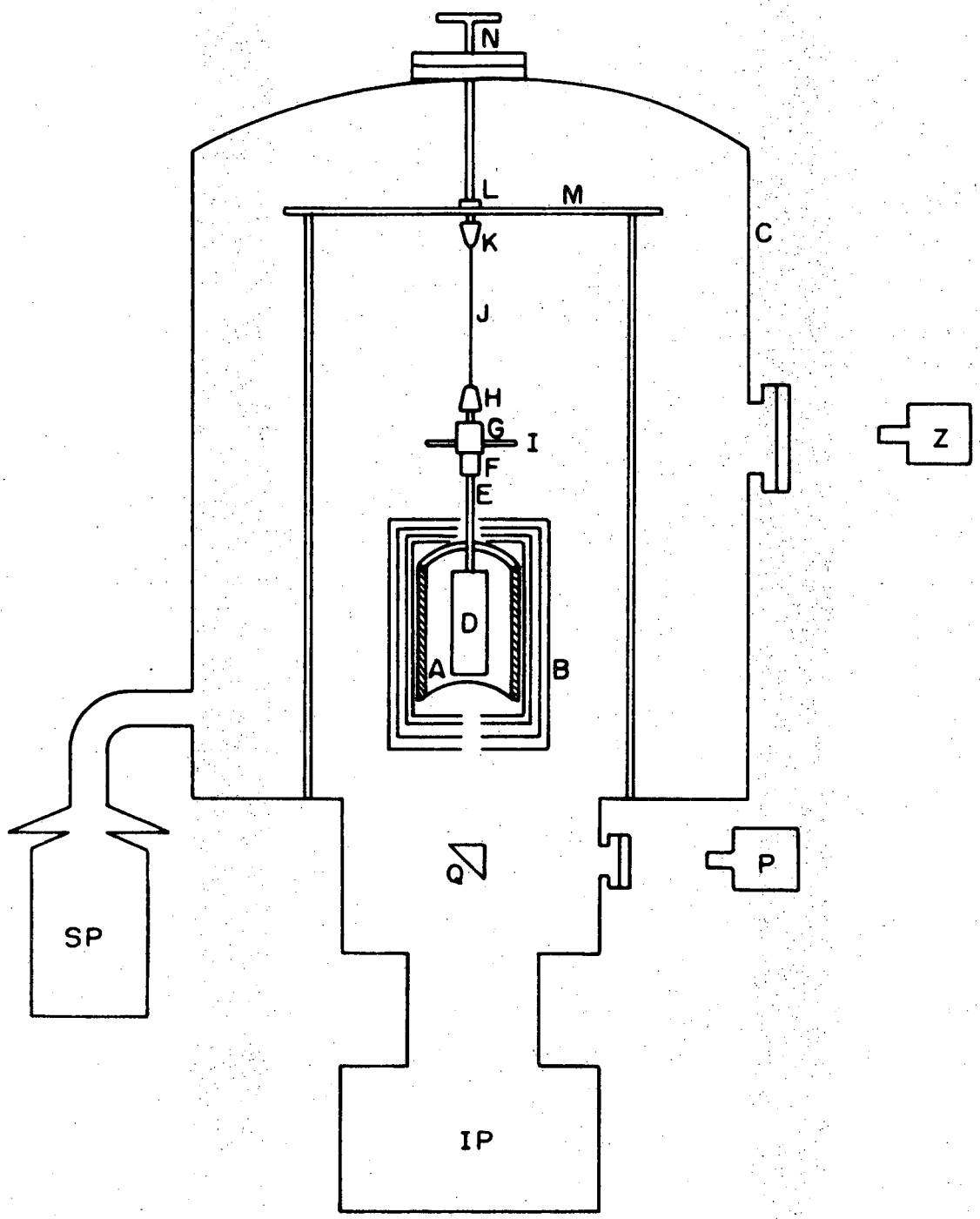

XBL 731 5639

Fig. 4. Sectional diagram of the experimental system.

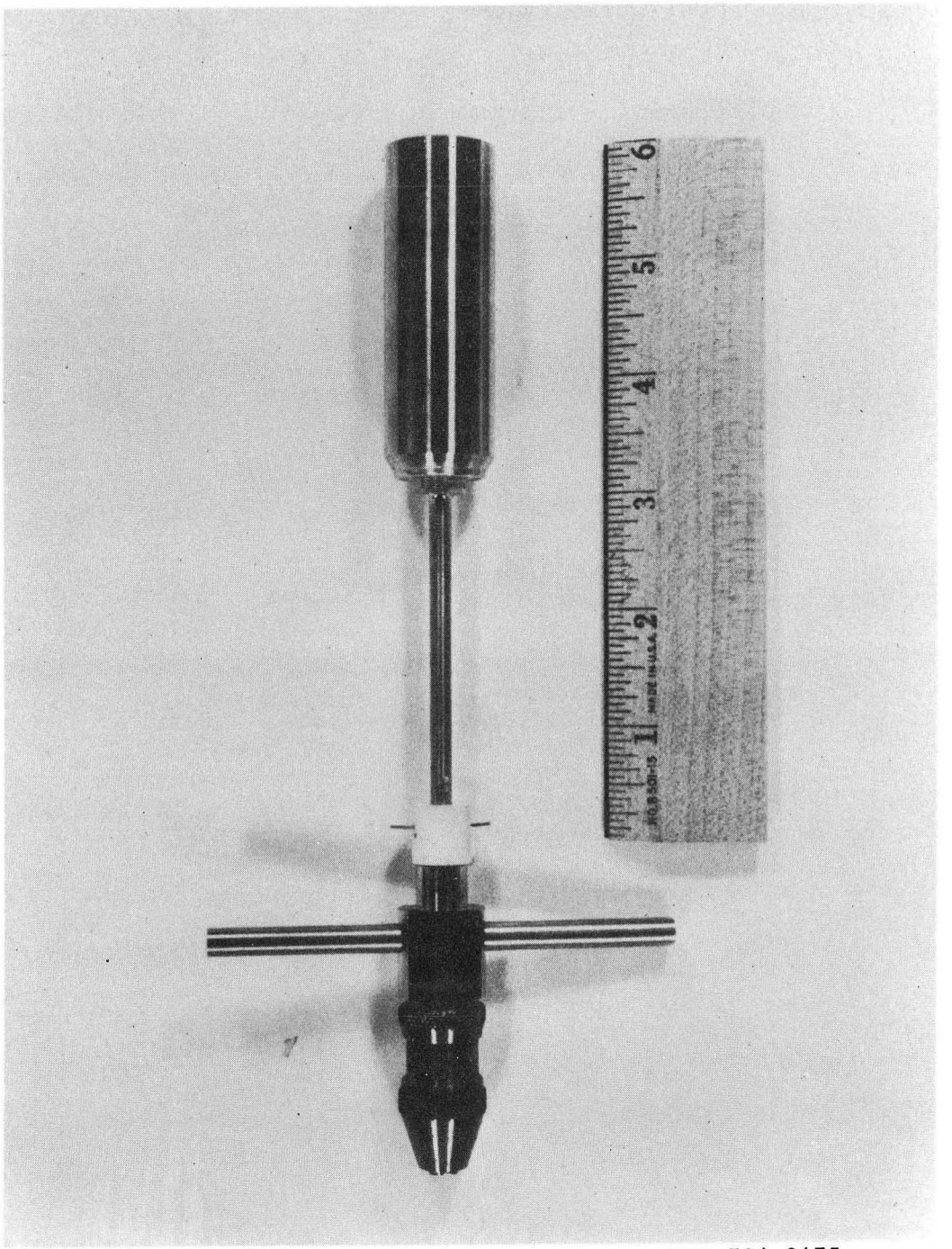

XBB 734-2475

Fig. 5. Torsion pendulum.

(P) which sighted through a right angle prism (Q) into a hole 1/8 inch in diameter drilled through the bottom shield parts into the inner furnace region is used to measure temperatures above 900°C.

The entire system is enclosed in a vacuum chamber (C) which serves three functions: 1) it prevents the oxidation at elevated temperatures, 2) it reduces heat loss by convection, 3) it minimizes damping effect due to the presence of surrounding gases.

To minimize absorption of the building vibrations, the entire apparatus is placed in a sand-filled pan.

B. Vacuum System

The system is equipped with a mechanical pump, an ion pump (IP) and two liquid nitrogen soprtion pumps (SP). To avoid vibrations, the mechanical pump is turned off when taking data. Instead of the ion pump, which is capable of maintaining the system at a lower pressure, the sorption pumps are used to keep the system vacuum at $< 3\times10^{-5}$ torr. This is done to eliminate the possibility of damaging the ion pump in case of a cesium leak from the crucible. The pressure maintained by the sorption pumps is low enough that no other pumping is necessary.

C. Pendulum Motion Recording System

The pendulum motion recording system is illustrated in Fig. 6 .

A helium gas laser is used as the incident light beam because of its strong intensity and spot size. The reflected light from the polished

surface on the pendulum triggers an 1N2175 photocell located in the vacuum chamber. Before feeding the output of the photocell into the multichannel analyzer, a logic circuit designed to correct the spatial error due to the finite dimension of the photocell and laser beam is employed. Due to the finite time required for the laser spot to pass the photocell, the output from the photocell has a certain width which increases as the oscillation motion slows down (Fig. 7). The logic circuit generates a narrow pulse each time when the laser beam passes the left edge of the photocell which is used as the reference position.

The corrected pulses are then sent as the channel advancing pulses to the multichannel analyzer operating in the multiscalar mode. At the same time, 100 KHz timing pulses are fed into the MCA. The counting starts at channel 1 and continues until a channel advancing pulse transfers the timing pulses to channel 2 and so on. Since each stored count is equivalent to 10 microseconds, the number of timing pulses stored in a particular channel provides an accurate measure of the time elapsed between successive passages of the beam past the photocell. Fig. 8 shows a typical set of data obtained in this manner.

The position of the photocell is in general different from the position of the reflected light beam with the pendulum in equilibrium (i.e., not oscillating). The upper points in Fig. 8 represent the time intervals for the pendulum to move from the photocell to the maximum angular displacement farthest from the photocell and return to the cell. The lower points are a similar record for the remaining portion of the oscillation. Figure 9 shows another version of the pendulum oscillation.

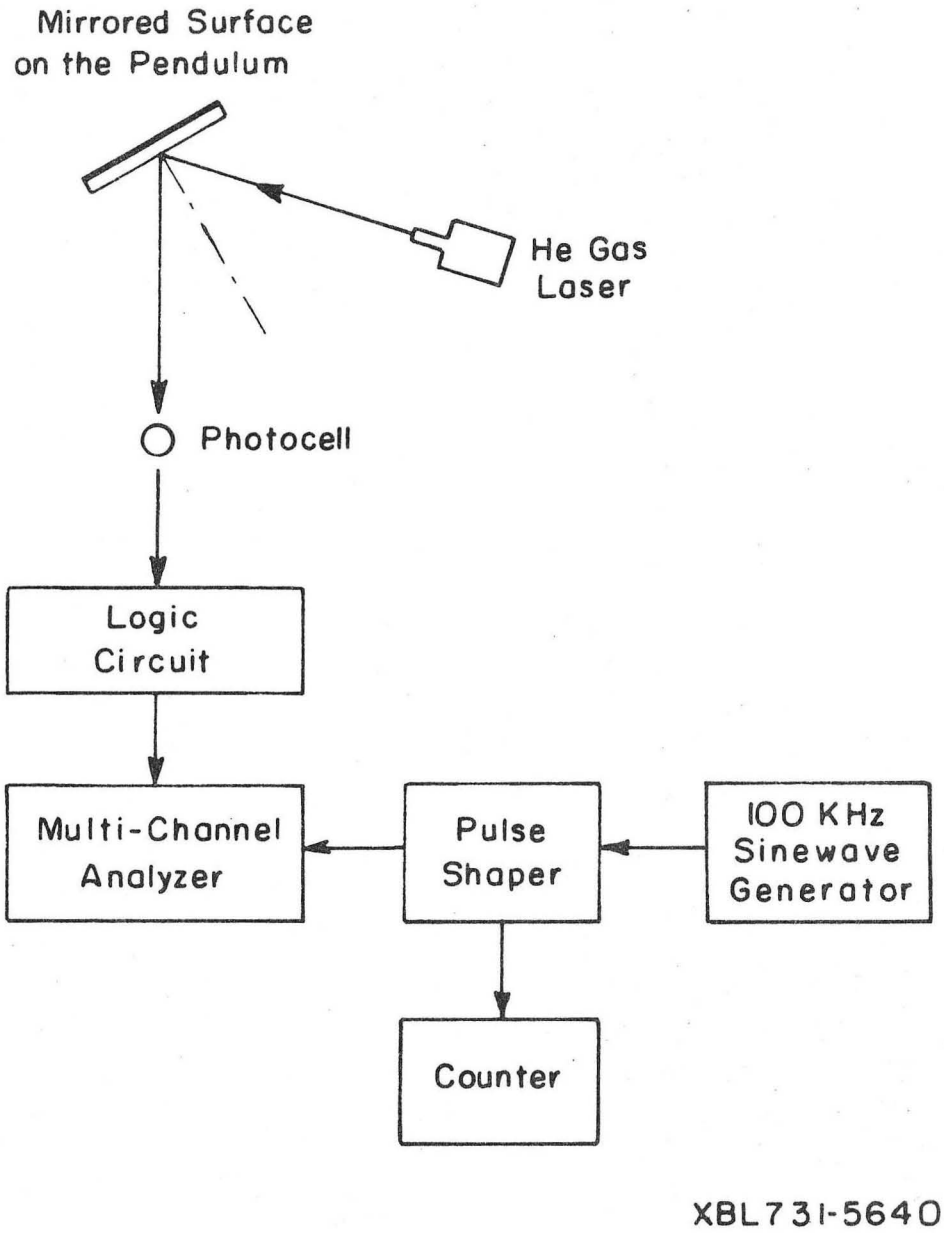

Fig. 6. Pendulm motion recording system.

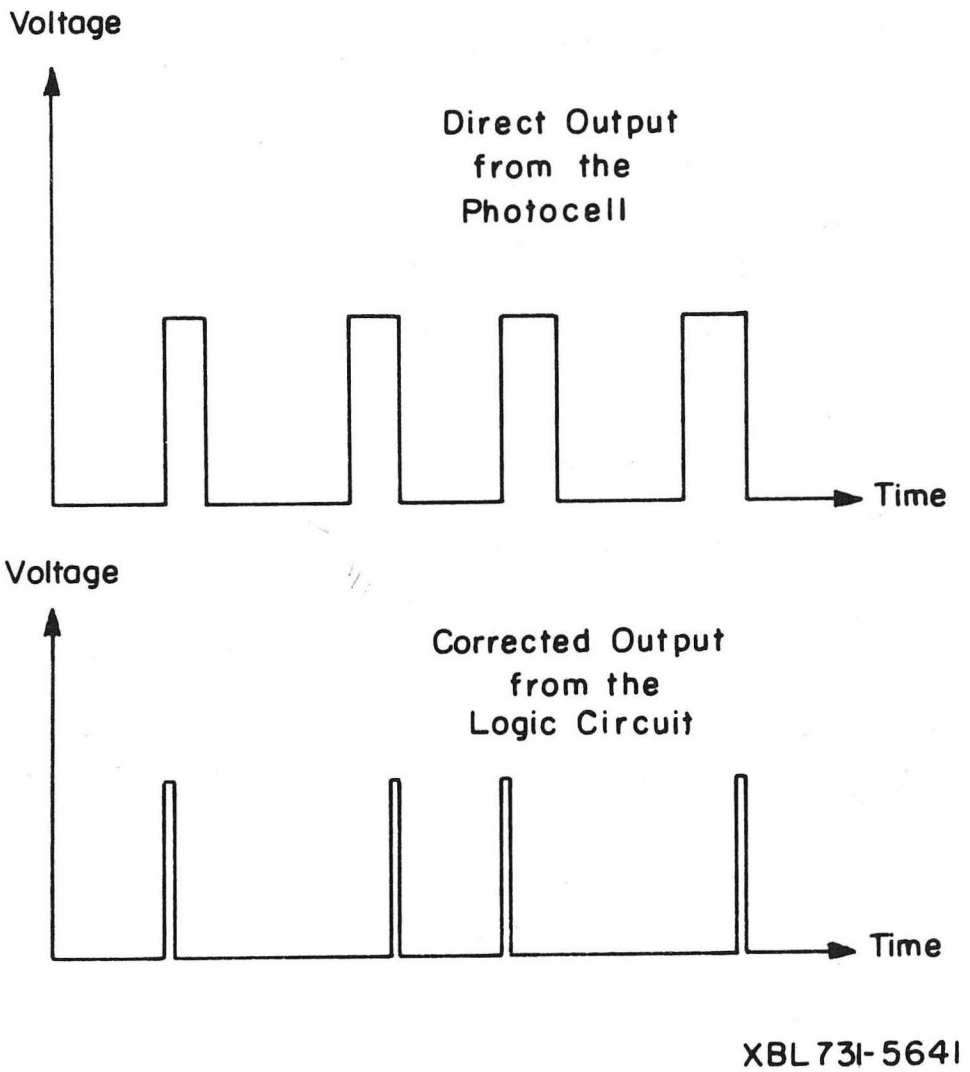

Fig. 7. The function of the logic circuit.

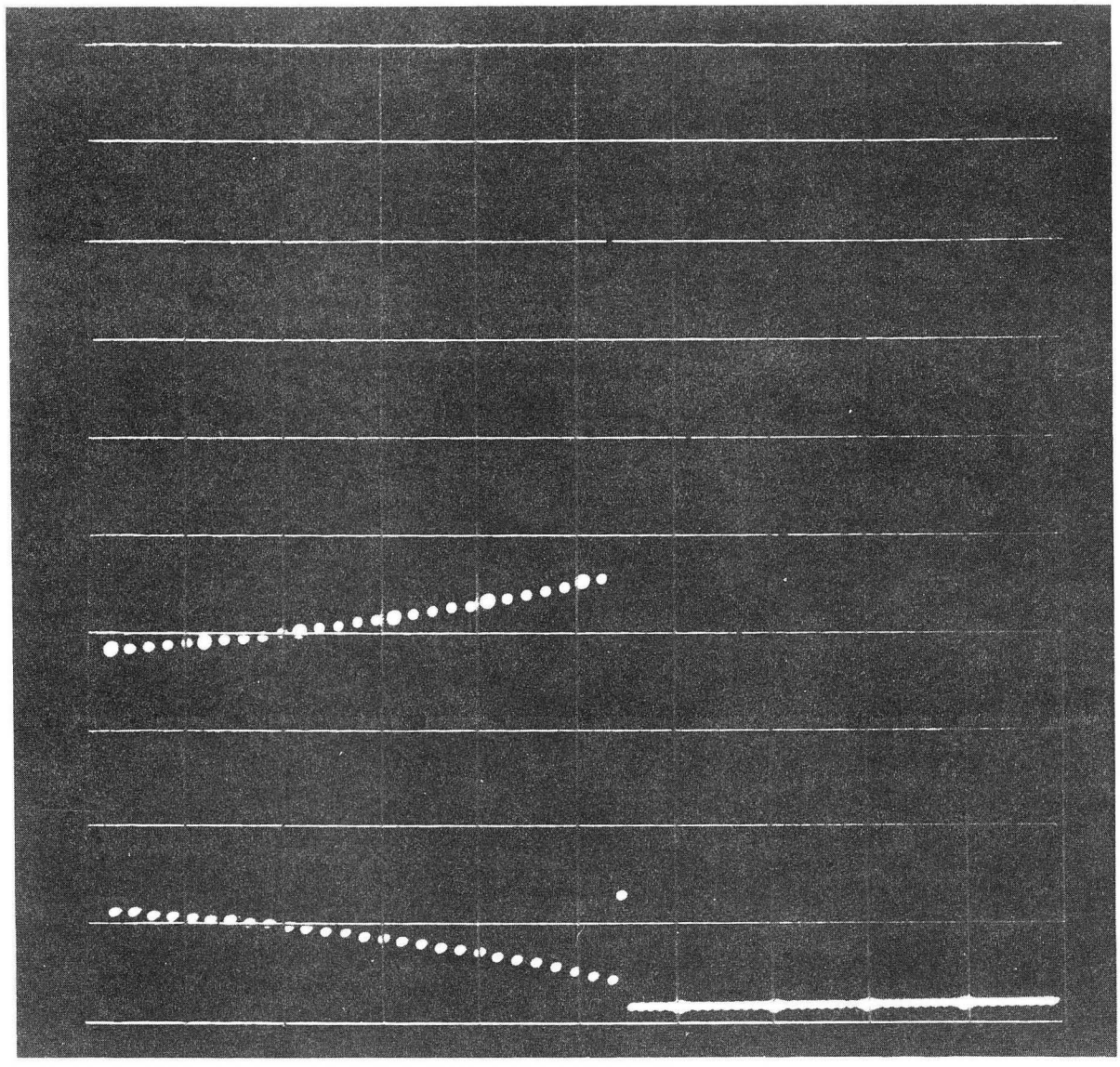

XBB 722-990

Fig. 8. A typical set of data shown on the screen of the multi-channel analyzer.

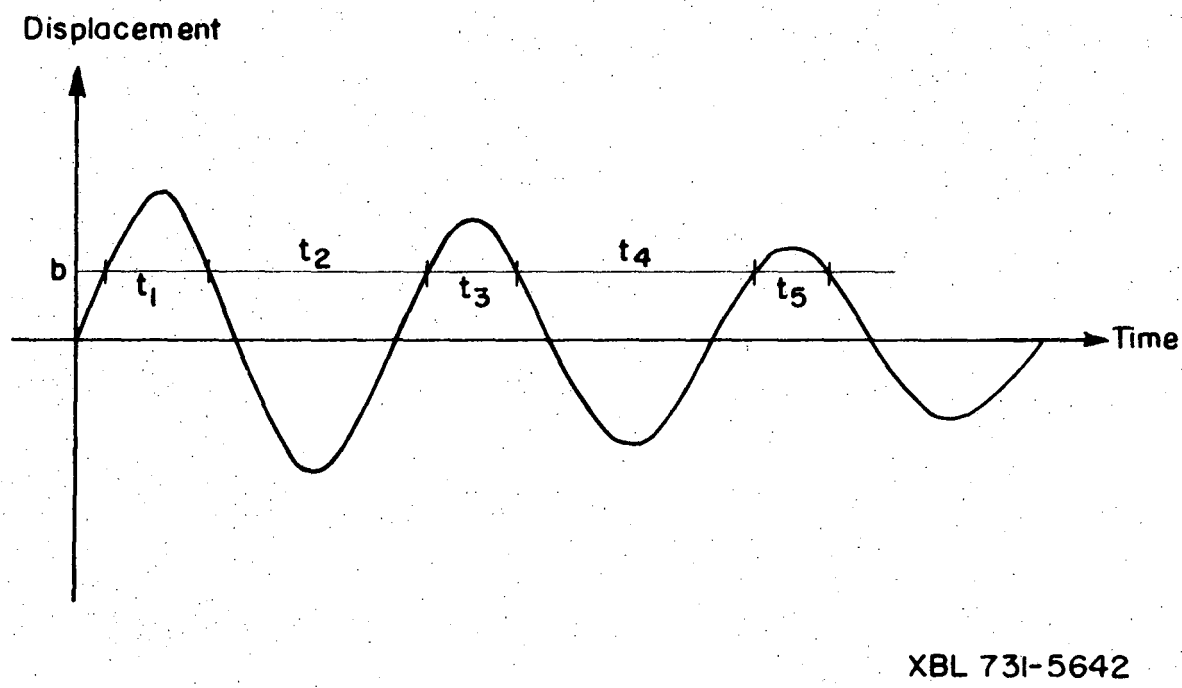

Fig. 9. The damped sinusoidal motion of the pendulum.

The damped sinusoidal curve represents the pendulum motion and the line b is the position of the left edge of the photocell. The points shown in Fig. 8 are the time intervals t_1, t_2, t_3, t_4, etc.

If the damping over the intervals t_1, t_3, t_5, etc. are small, the curve in Fig. 9 can be considered as symmetric around each of the peaks. The heights of the peaks are then proportional to the inverse of $\cos\frac{\pi t_1}{\tau}$, $\cos\frac{\pi t_3}{\tau}$, etc., where τ is the period. Therefore the decay constant β, by definition, is

$$\beta = \frac{1}{2\pi} \ln\left[\frac{\cos\left(\frac{\pi t_3}{\tau}\right)}{\cos\left(\frac{\pi t_1}{\tau}\right)}\right]$$

If the asymmetry of the pulses is taken into account the percentage error can be shown to be less than[22]

$$\frac{x_3 - x_1}{4\pi}$$

where

$$x_3 = \frac{\pi t_3/\tau}{\tan\left(\frac{\pi t_3}{\tau}\right)}$$

$$x_1 = \frac{\pi t_1/\tau}{\tan\left(\frac{\pi t_1}{\tau}\right)}$$

which in the present experiments, is always less than 0.1%.

D. Torsion Wire Preparation

In measuring the damped sinusoidal motion of a oscillating cup viscometer, some degree of damping is always observed even when the sample is in solid form. This inherent damping is mainly due to the presence of the internal friction in the torsion wire. There are many explanations of the causes of the internal friction,[23,24] the most significant ones being dislocation line movement and grain boundary slip. Impure polycrystalline metals normally have less internal friction than high purity specimens because the impurities effectively pin the dislocation lines. Annealing is also effective in reducing the internal friction because it reduces the density of dislocation line and, depending on annealing temperature, reduces the total grain boundary area. For these reasons, annealed 3% Re-W wire was chosen as the torsion fibre.[25] Figure 10 shows the difference between pure tungsten and 3% Re-W wires and the effectiveness of annealing.

E. Tungsten Crucible Design

The vapor pressure of cesium increases sharply when the critical temperature is approached (Fig. 1). On the other hand, the strength of tungsten decreases rapidly with temperature.[26] Special precautions therefore, have to be taken in designing the crucibles for high temperature, high pressure experiments. Tungsten was chosen over tungsten alloys which have higher yield stress because of its good corrosion resistance.[13]

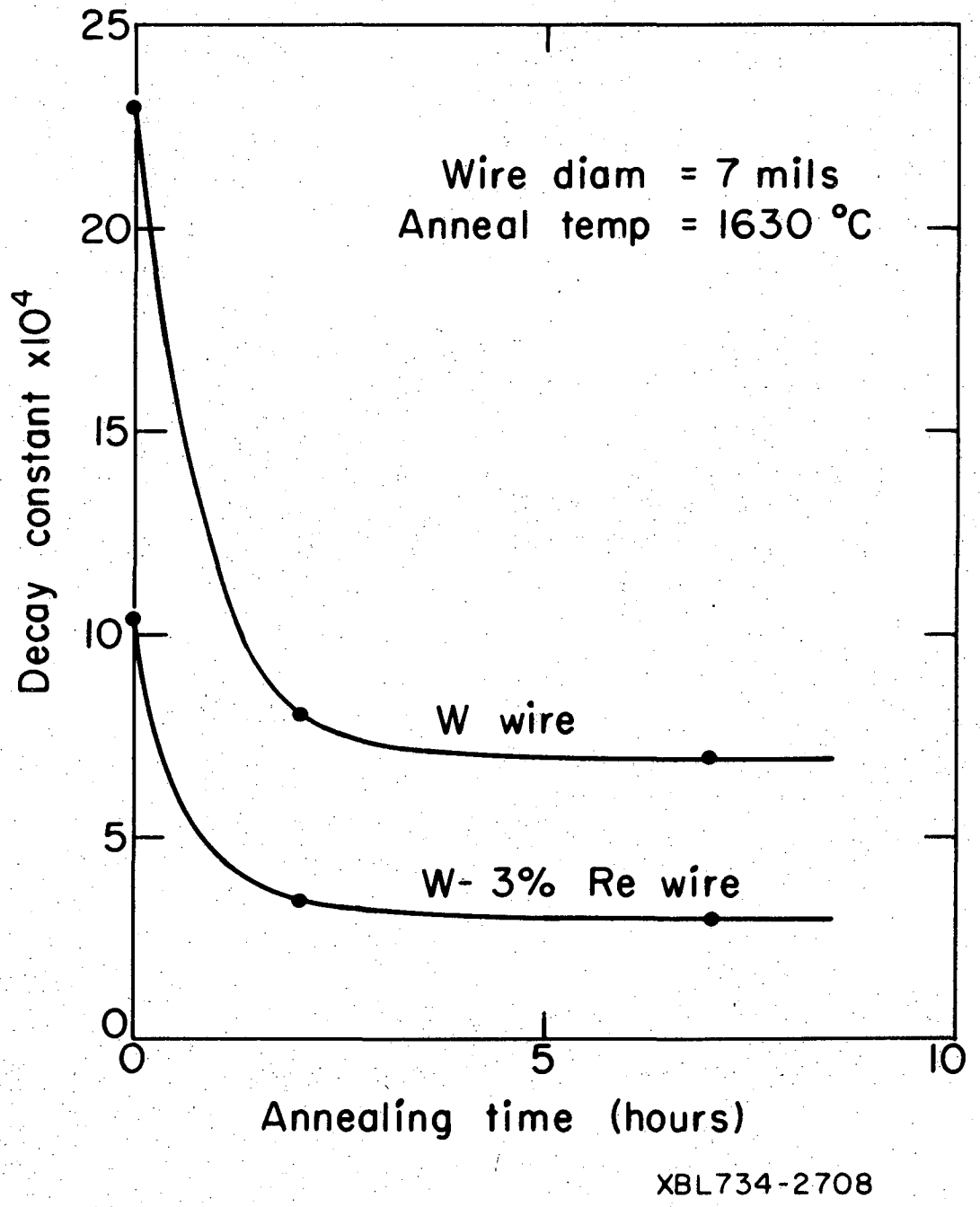

Fig. 10. Effectiveness of impurity and annealing on the internal friction of torsion wire.

Two kinds of crucible were used in this research. The "thin-wall" ones shown in Fig. 11 were used for lower temperature runs. Figure 12 is the sectional view of the "pressure vessel" type crucibles used for high temperature, high pressure runs.

All the crucibles were fabricated from forged tungsten rod stock by Northwest Industries, Inc. Prior to the loading of cesium, the crucibles were vacuum annealed at 1000°C for 20 minutes. This procedure relieves the internal stress introduced in machining and helps prevent cracking when the lids were later sealed by electron-beam welding. Vacuum annealing at this temperature is also an effective way to clean tungsten.

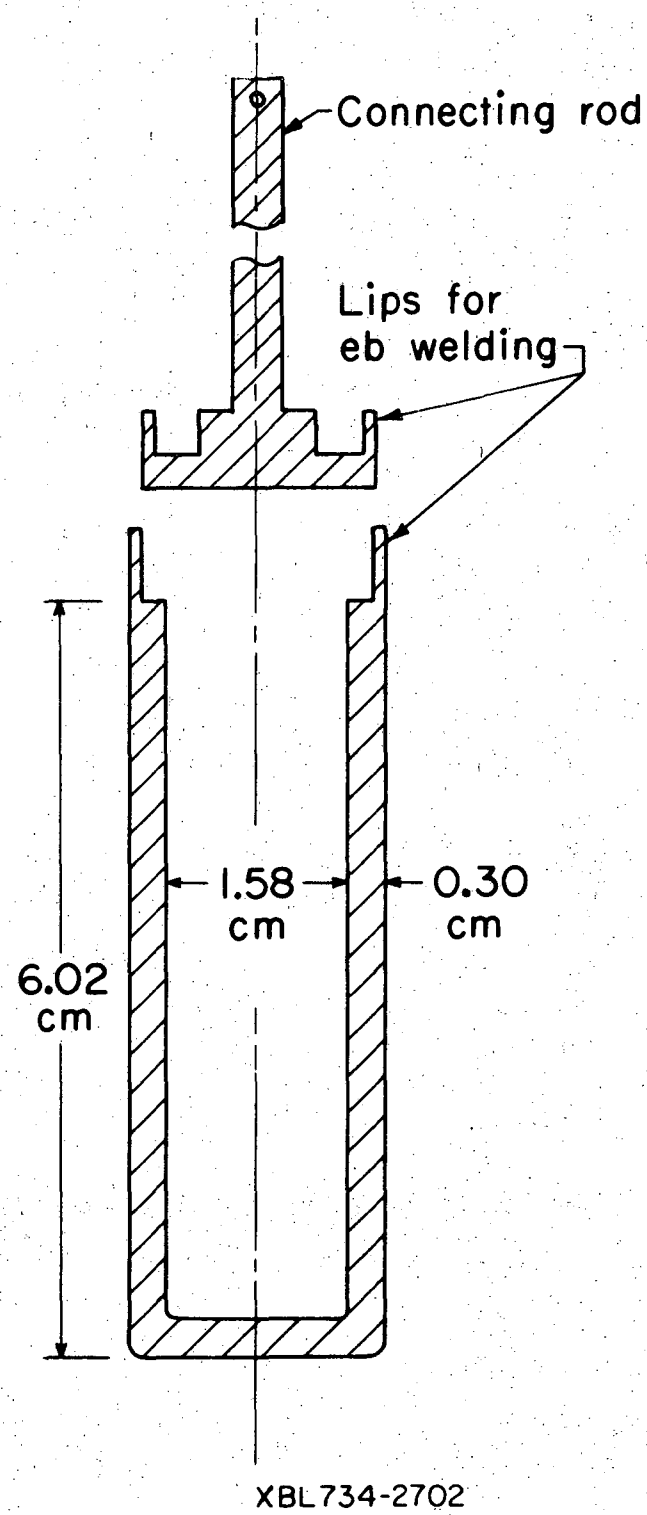

Fig. 11. Sectional view of the thin-wall crucible.

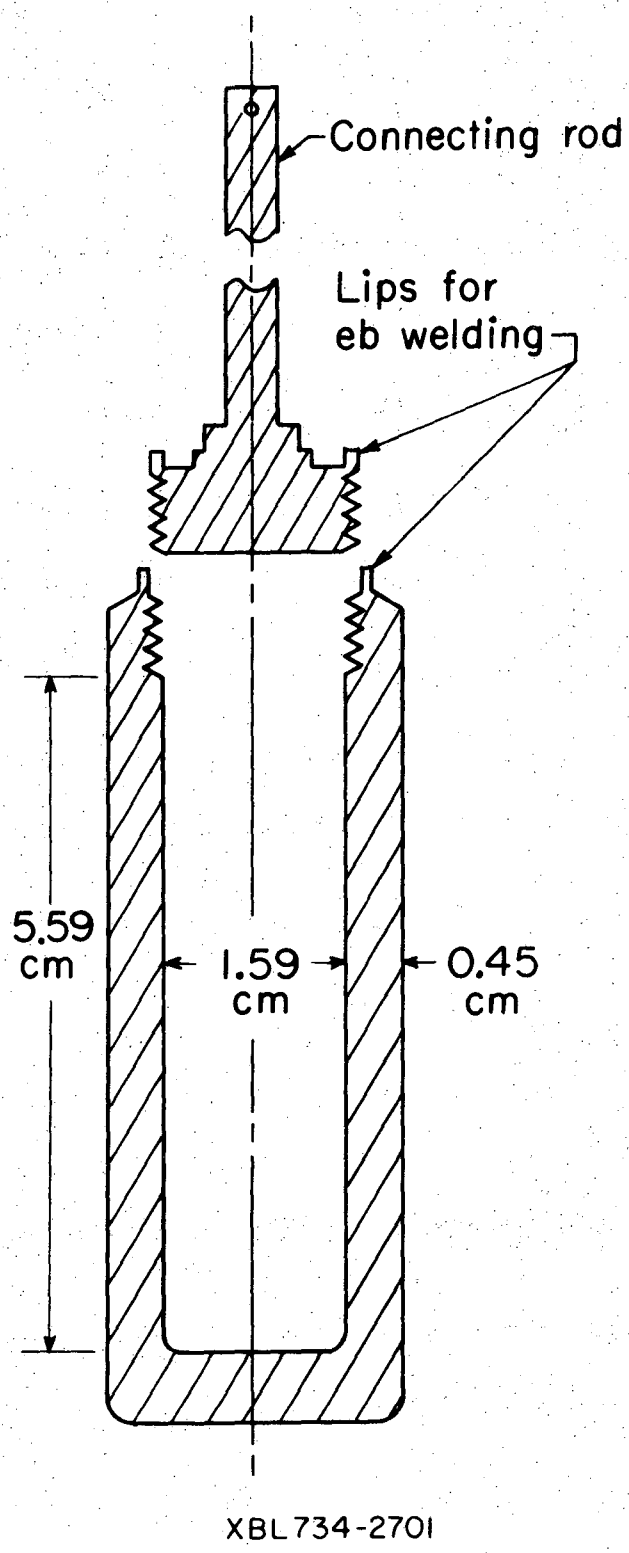

Fig. 12. Sectional view of the thick-wall crucible.

IV. EXPERIMENTAL PROCEDURE

A. Sample Preparation

The high purity (99.99%) cesium metal used in this research was supplied by Leico Industries, Inc. A typical chemical analysis of the sample is shown in Table II.

Tungsten crucibles and cesium sealed in glass ampoules were loaded in a glove box flushed with dry nitrogen. The cesium was heated to the melting point and poured into the crucible. The amount loaded was roughly controlled by measuring the weight increase of the crucible using the balance inside the glove box. After the lid was electron-beam welded to the body, the exact weight of the cesium charge was accurately measured by an analytic balance.

To prevent overheating of the cesium metal during electron beam welding, the crucible was held in a cylindrical copper block (9 cm diameter by 13 cm height) with a central hole to hold the crucible. In order to serve as a heat sink, the copper block was prechilled to liquid nitrogen temperature. This method effectively eliminated the vaporization of cesium during the welding operation but increased the possibility of cracking in the weld due to the large thermal gradient.

Transfer of the loaded crucible from the glove box into the electron beam welder was done in less than 10 seconds. Since the loaded crucibles were chilled to liquid nitrogen temperature before leaving the glove box, gas flow through the tight-fitting lids (if any) would be from the inside

Table II. Chemical Analysis of Cs Sample

Impurities	Content (ppm)
Aluminum	< 2
Calcium	< 5
Chromium	< 2
Copper	< 2
Iron	< 5
Lead	< 2
Lithium	<10
Magnesium	< 2
Manganese	< 2
Nickel	< 2
Potassium	< 8
Rubidium	< 8
Silicon	< 3
Sodium	< 8

out as the crucible warmed up. Thus it is believed that the cesium did not become oxidized during the short period of transportation from the dry box to the welder and the pump-down time of the vacuum system of the welder.

B. Moment of Inertia Measurement

In order to determine the viscosity from the decay constant measurements, the moment of inertia of the pendulum system is required. This quantity is determined by comparing the oscillation periods of the pendulum with and without an attached rod of known moment of inertia.

Let I_o be the moment of inertia of the system without the inertia rod, the period T_o for small amplitude oscillation is

$$T_o = 2\pi\sqrt{\frac{I_o}{f}} \tag{38}$$

where f is the spring constant of the torsion wire. By attaching the rod with known moment of inertia I_b to the pendulum, the period increases to

$$T_1 = 2\pi\sqrt{\frac{I_o+I_b}{f}} \tag{39}$$

Therefore I_o can be determined from (38) and (39) as

$$I_o = \frac{I_b}{\left(\frac{T_1}{T_o}\right)^2 - 1}$$

In the actual analysis, however, the moment of inertia of the system excluding the sample is used. The calculated inertia of the solid sample therefore has to be subtracted from I_o.

C. Viscosity Measurement

Since the system has been previously tested on liquid tin and been used to measure the viscosities of uranium metal[22] and uranium dioxide,[27] no further verification of the system accuracy has been made for the present experiment.

The intrinsic damping effect was measured before each experiment when the sample was in solid form. The temperature of the hot zone was then gradually increased while the pressure gauge was closely monitored for any cesium leakage. At each temperature, sufficient time was allowed for the crucible to reach thermal equilibrium with the hot zone. A braking device was then engaged to bring the pendulum system completely to rest before an initial twist was transmitted to the pendulum through the rotational feedthrough on top of the vacuum chamber. In each experiment, 25 consecutive oscillations were recorded and used to determine the mean period and decay constant.

After the experiments were over, the intrinsic decay constant was measured again to reaffirm the value measured prior to the experiments. The temperature dependence of the intrinsic damping was determined separately with a dummy crucible (consisting of solid tungsten). β was found to be independent of temperature in the experimental range.

V. RESULTS

The cesium viscosity measurements were carried out with two thin-wall crucibles (A and B) in the temperature range from 135 to 550°C and from 530 to 815°C, respectively, and with one pressure vessel type crucible (D) from 800 to 1600°C. Slight overlap of the temperature ranges provided a check of the consistency of data obtained from different viscometers. The information on these three viscometers is given in Table III.

Two-phase solution was employed for temperatures greater than 600°C, at which temperature the reported vapor viscosity is about 1/8 of that of the liquid. The saturated cesium vapor viscosities used in the two-phase solution were taken from the work of Bonilla et al.[28]

Figures 13 and 14 show the measured cesium viscosity plotted as η vs. T and log η vs. 1/T, respectively. The data are also tabulated in Table IV. Achener and Boyer[29] have measured the cesium viscosity using the oscillating cup technique up to 1060°C. Their result is shown in Fig. 13 for comparison. The agreement between their results and the present data is quite good.

The difference between the values of the liquid viscosity deduced from the set of data points but analyzed by the single-phase and two-phase solutions of the equations of motion depends on the temperature and the relative height of the vapor phase compared to that of the liquid. With viscometer B, at 600°C the corrected liquid viscosity is 8% less than that without the correction for vapor drag. For crucible D at 1600°C the analogous figure is 30%.

Table III. Characteristics of Viscometers and Cesium Charges

	Viscometer A	Viscometer B	Viscometer D
Crucible Type	thin wall, tungsten	thin wall, tungsten	pressure vessel, tungsten
Crucible I.D. (cm)	1.58	1.58	1.59
Crucible inside Height (cm)	6.05	6.04	5.59
Moment of Inertia ($gm\text{-}cm^2$)	274.62	275.84	397.33
Torsion Wire	W-3% Re, 7 mil, annealed	W-3% Re, 7 mil, annealed	W-3% Re, 7 mil annealed
Cesium Charge (gms)	15.593	10.035	7.044
Height of Liquid (cm)	4.44 at 500°C	3.68 at 815°C	4.05 at 1605°C
Temperature Range	135-550°C	530-815°C	800-1605°C

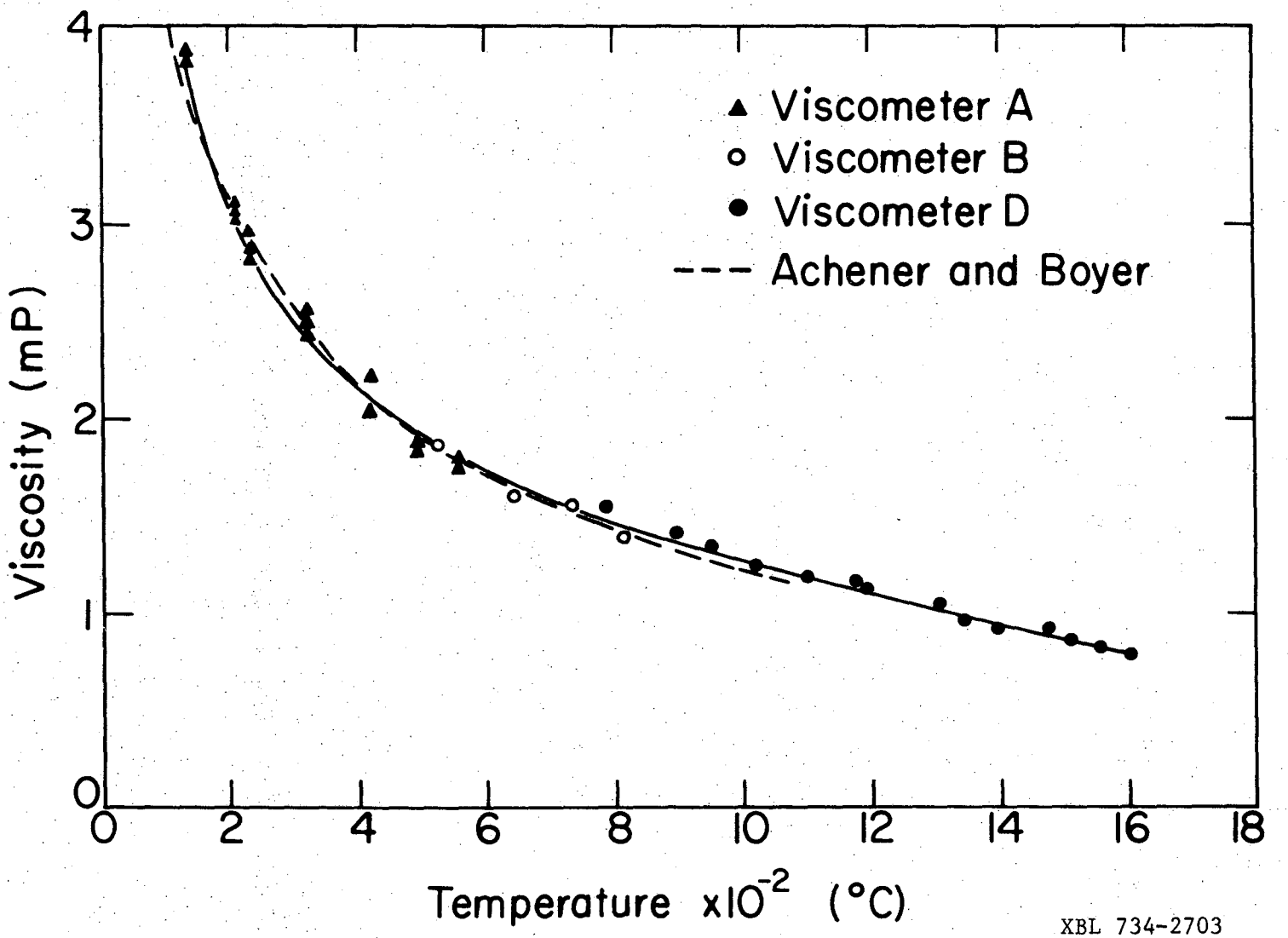

XBL 734-2703

Fig. 13. Liquid cesium viscosity.

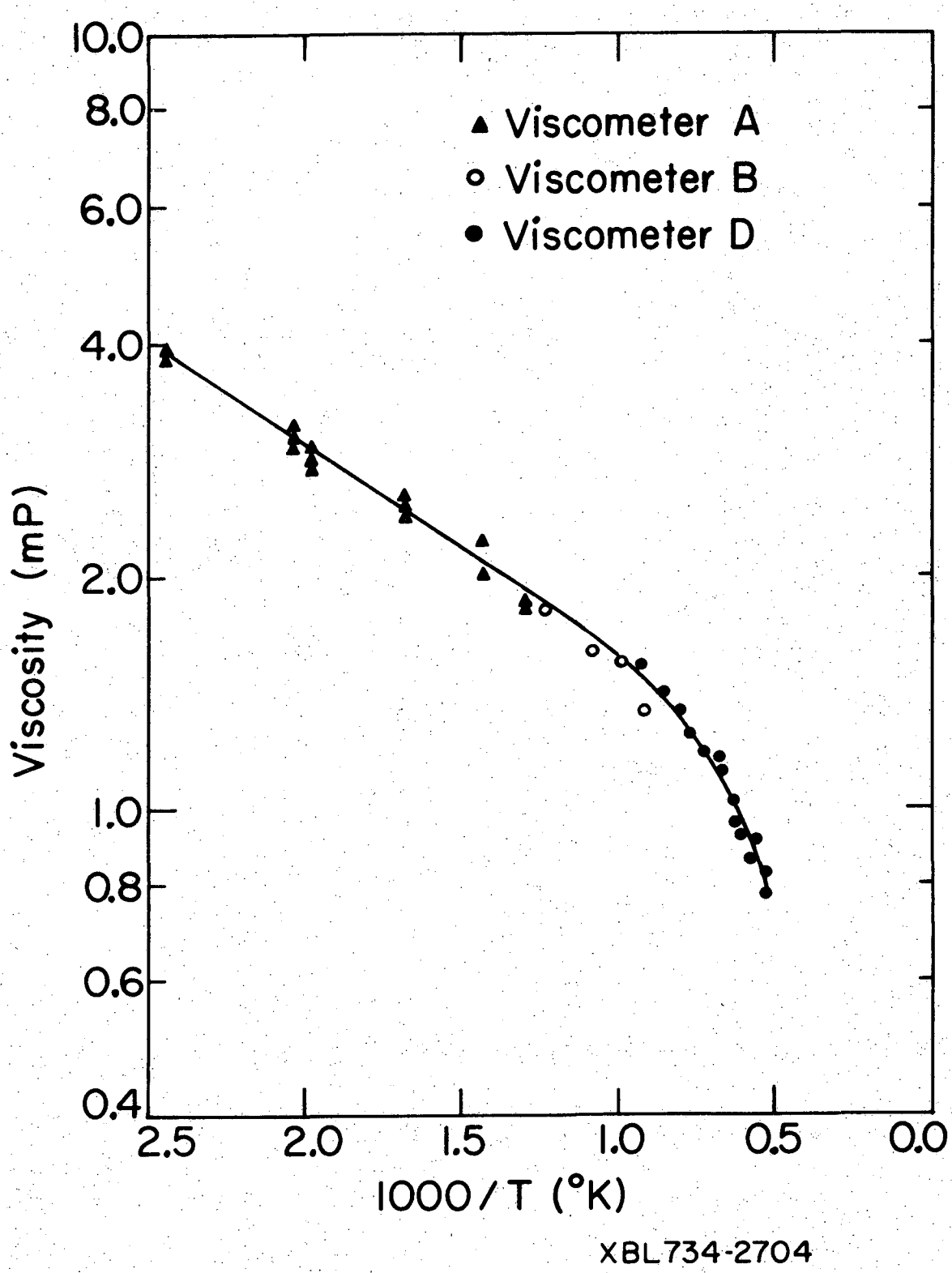

Fig. 14. Liquid cesium viscosity.

Table IV. Cesium Viscosity Data

Temperature (°C)	Period (seconds)	Decay Constant (10^{-3} sec^{-1})	Vapor Viscosity (millipoise)	Liquid Viscosity* (millipoise)
135	3.175	1.718	-	3.86
135	3.216	1.712	-	3.89
216	3.174	1.558	-	3.06
216	3.215	1.551	-	3.08
216	3.174	1.542	-	3.00
232	3.175	1.538	-	2.96
232	3.217	1.491	-	2.81
232	3.219	1.498	-	2.84
320	3.181	1.438	-	2.49
320	3.181	1.496	-	2.52
320	3.221	1.412	-	2.43
420	3.185	1.321	-	2.02
420	3.184	1.378	-	2.21
497	3.183	1.282	-	1.84
497	3.183	1.295	-	1.88
556	3.185	1.281	-	1.80
556	3.185	1.279	-	1.79
645	3.24	0.919	0.22	1.59
735	3.24	0.918	0.24	1.53
815	3.24	0.880	0.26	1.41
790	3.94	0.424	0.25	1.54
898	3.92	0.420	0.27	1.41
957	3.94	0.415	0.28	1.34
1024	3.92	0.412	0.29	1.25
1105	3.94	0.411	0.31	1.20
1183	3.92	0.415	0.32	1.15
1197	3.94	0.410	0.32	1.12

Table IV. Continued

Temperature (°C)	Period (seconds)	Decay Constant (10^{-3} sec^{-1})	Vapor Viscosity (millipoise)	Liquid Viscosity* (millipoise)
1308	3.94	0.406	0.34	1.02
1348	3.92	0.403	0.35	0.97
1400	3.93	0.402	0.36	0.93
1472	3.92	0.407	0.37	0.91
1510	3.94	0.402	0.38	0.87
1555	3.92	0.402	0.39	0.83
1605	3.94	0.400	0.39	0.79

* Corrected for vapor viscosity for T > 600°C.

The measured Cs liquid viscosity was fitted by the equation

$$\ln \eta = -0.187 + \frac{6.34\times10^2}{T}, \quad 410°K \leq T \leq 1100°K$$

$$\ln \eta = -2.55 + \frac{6.01\times10^3}{T} - \frac{3.10\times10^6}{T^2}, \quad 1100°K < T < 1900°K$$

where η is the dynamic viscosity in millipoises and T is the absolute temperature in °K. The standard deviation of the viscosity for the above two expressions are 0.008 mP and 0.06 mP, respectively.

The activation energy for the low temperature range is 1.3 ± 0.2 kcal/gm-mole. The values found by Achener and Boyer[29] are 1.03 kcal/gm-mole for the 55 to 448°C range and 1.76 kcal/gm-mole for the 533 to 1064°C range. The liquid viscosity does not follow an Arrhenius law in the high temperature range, so cannot be characterized by a single activation energy.

VI. DISCUSSION

A. Law of Rectilinear Diameters: The Critical Viscosity of Cesium

It was first discovered by Cailletet and Mathias in 1886 that when approaching the critical temperature, the mean density of the liquid and its saturated vapor is approximately a linear function of temperature.[30] This is the so-called law of rectilinear diameters. Grosse later pointed out that this law also applies to liquid and vapor viscosities.[11]

The fact that the viscosity varies rapidly as the critical temperature is approached coupled with the problem of loading exact amount of sample into a constant volume device like the oscillating crucible makes the direct measurement of critical viscosity very difficult. Like most of the critical density measurements, law of rectilinear diameters was utilized to estimate the critical viscosity of the cesium metal by extrapolating data at lower temperatures. Since the present data extend quite close to the critical point, the accuracy of such an extrapolation is good.

The mean viscosity $\bar{\eta}$ is calculated and shown in Fig. 15. The data between 1200 to 1600°C were least-squares fitted into a straight line

$$\bar{\eta} = \tfrac{1}{2}(\eta_{liq.} + \eta_{sat.vap.}) = 1.13-3.21\times10^{-4}T$$

where T is the temperature in °C. The mean viscosity in this temperature range is a very good linear function of temperature. Extrapolating the mean viscosity to 1760°C, the reported critical temperature of cesium,[12]

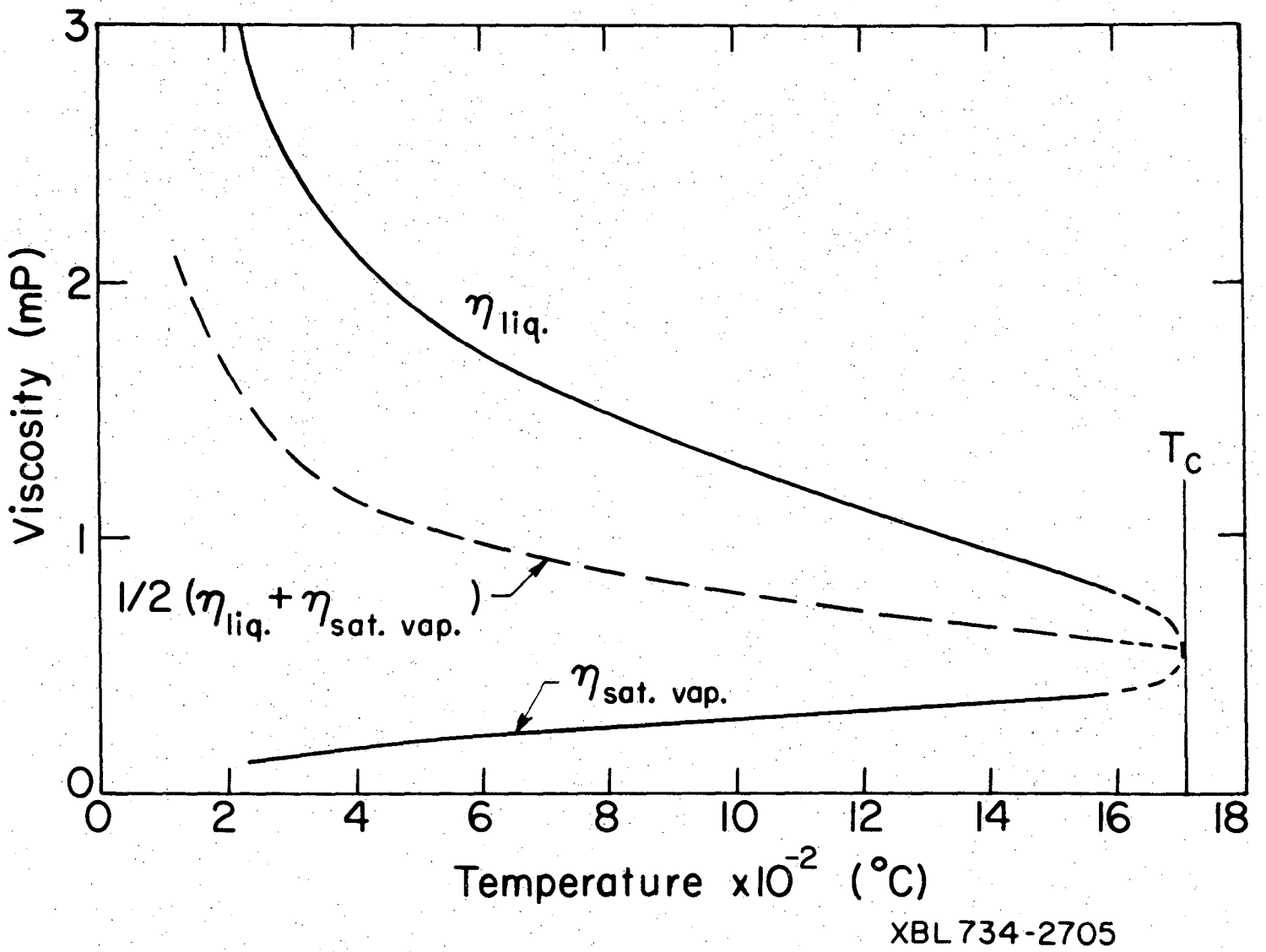

Fig. 15. Law of rectilinear diameters of cesium metal.

yields a critical viscosity of 0.57 ± 0.4 millipoises. This value is smaller than the 0.8 millipoises Grosse obtained by extrapolation of estimated sodium and potassium critical viscosities.[11]

B. Andrade's Theory of Liquid Viscosity[31]

Consider a simplified model of the liquid state in which the molecules are arranged in a regular array and are in constant vibrational motion. In order for a molecule to jump to an adjacent site to which the momentum is transferred by virtue of a velocity gradient, an energy E_o to overcome the potential barrier is required. According to the Boltzmann distribution law, the ratio of number of molecules possessing energy E_o at temperatures T to the number possessing this energy at temperature T' is

$$e^{\frac{E_o}{k}\left(\frac{1}{T} - \frac{1}{T'}\right)}$$

This is the main factor in the temperature dependence of viscosity, for which an approximate formula is

$$\eta_T = \eta_{T'} e^{-\frac{E_o}{kT'}} e^{\frac{E_o}{kT}} = A\, e^{Eo/kT} . \qquad (40)$$

This is the so-called Andrade I equation.

In deriving the above equation, no account was taken of the variation of liquid specific volume with temperature. The average distance between molecules increases with temperature as $V^{\frac{1}{3}}$, where V is the specific volume, and the number of molecules per unit area diminishes as $V^{-\frac{2}{3}}$.

From the mean field theory of the classical van der Waals model,[32] E_o can be taken as a/V where a is a constant. The result is the Andrade II equation:

$$\eta V^{\frac{1}{3}} = A\ e^{a/VT} \tag{41}$$

The measured cesium viscosity was tested against these two predictions. In Fig. 14 data are plotted according to the first equation. It can be seen that the measured cesium data are in good agreement with Eq.(40) up to 1000°K. Beyond that, the data start to deviate from the predicted straight line. Comparison of cesium data with the Andrade II equation is shown in Fig. 16. Again, cesium behaves as predicted only in the low temperature region. This is not surprising since the equations were derived based on the assumption of lattice structure of the liquid. This model fails at high temperature, however, since the molecules possess high kinetic energies and tend to make the liquid structure more random than solid-like.

C. Theory of Corresponding States: Viscosities of Sodium and Potassium

The high pressure limitation discussed in the Introduction is the reason that the entire liquid range of the alkali metals might not be covered experimentally for some time to come. Because of their high critical pressure, lithium, sodium and potassium are even more difficult to contain near the critical point than is cesium. Consequently it is desirable to estimate the critical viscosity of the other alkali metals from the measured cesium data by using the theory of corresponding states.

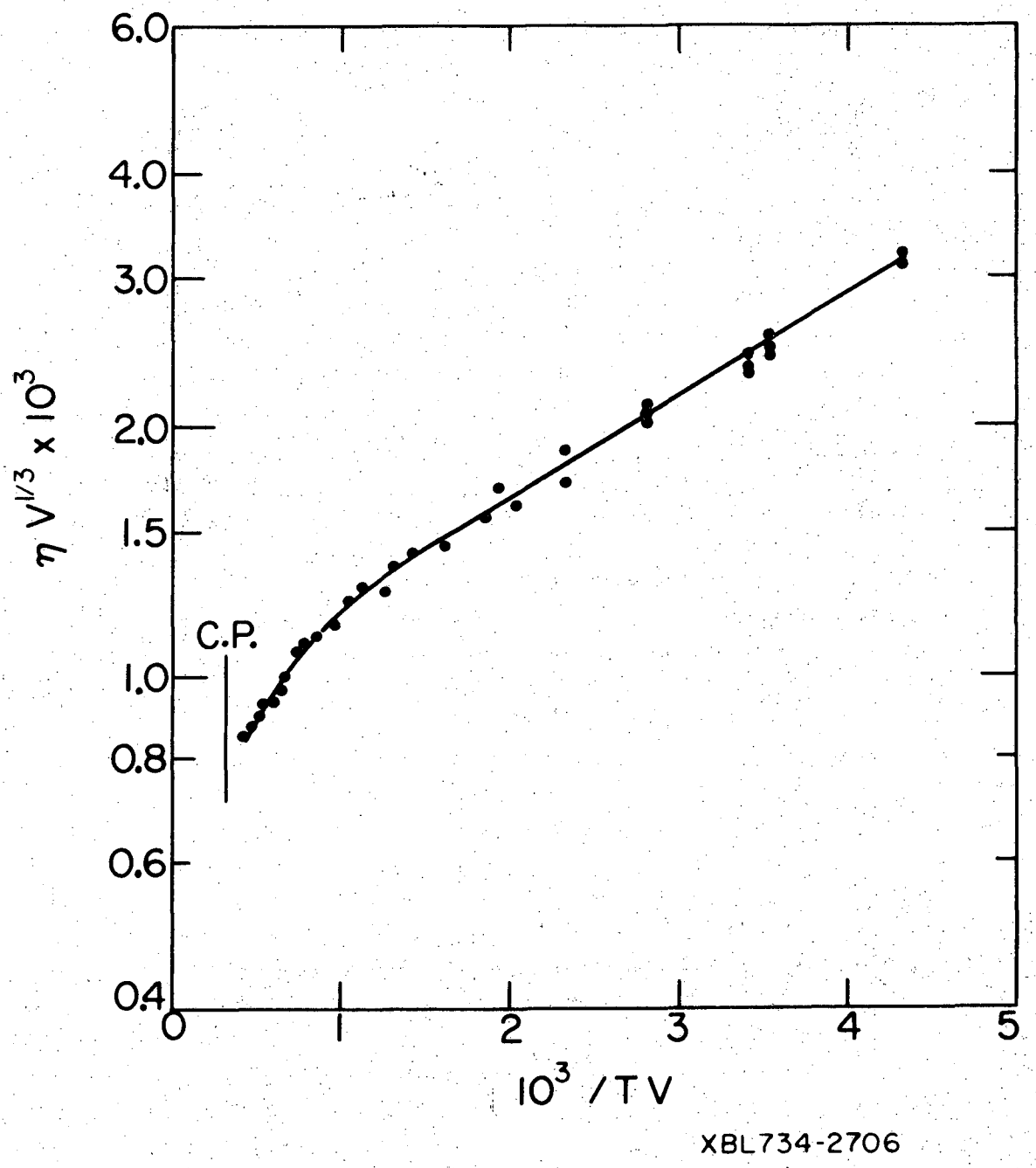

Fig. 16. Cesium viscosity in the form of Andrade II equation.

One of the conditions for the validity of the principle of corresponding states is that the reduced potential energy between molecules be written as a universal function of the reduced intermolecular distance (e.g., $\frac{u}{\varepsilon} = u(\frac{r}{\sigma})$, where ε and σ are the force constants of the potential function). The similarity in the properties of the alkali metals should satisfy this requirement quite well. It can be shown that with this condition, a law of corresponding states for viscosity can be derived.[33,19] The reduced viscosity is

$$\eta^* = \eta^* (T^*,V^*) = \frac{\eta\sigma^2 N_o^{\frac{1}{2}}}{M^{\frac{1}{2}}\varepsilon^{\frac{1}{2}}} \tag{42}$$

where T^* = reduced temperature = $\frac{kT}{\varepsilon}$

V^* = reduced volume = $\frac{1}{n\sigma^3}$

n = molecular density

M = molecular weight

N_o = Avogadro's number.

Because of the difficulty of finding the necessary values for σ, it is convenient to follow Pasternak's method[20] of multiplying η^* by $(V^*)^{\frac{2}{3}}$ to eliminate σ from Eq.(42). The resulting dimensionless quantity is

$$\eta^*(V^*)^{\frac{2}{3}} = \frac{\eta N_o^{\frac{1}{3}} V^{\frac{2}{3}}}{(MR\frac{\varepsilon}{k})^{\frac{1}{2}}} = f(T^*) \tag{43}$$

where R is the gas constant. The energy parameter $\frac{\varepsilon}{k}$ in Eq.(43) is determined from the empirical relationship found by Chapman:[19]

$$\frac{\varepsilon}{k} = 5.2\ Tm \tag{44}$$

where Tm is the melting point of the liquid metal in degrees Kelvin.

In Fig. 17, $\eta^*(V^*)^{\frac{2}{3}}$ vs. T^* is plotted from the measured cesium viscosity. The sodium and potassium viscosities predicted from the universal plot of Fig. 17 are shown in Figs. 18 and 19, respectively, along with the experimentally measured results of Kalakutskaya.[34] The agreement is satisfactory at medium and high temperatures. With the vapor viscosity data provided by Bonilla and co-workers, law of rectilinear diameter may be used to determine the following critical viscosities:

$$\eta_c = 0.50 \pm 0.5 \text{ millipoise} \quad \text{for sodium}$$

and

$$\eta_c = 0.46 \pm 0.5 \text{ millipoise} \quad \text{for potassium .}$$

The reduced viscosity of the alkali metals at the critical point is:

$$\eta_c^* = 0.24 .$$

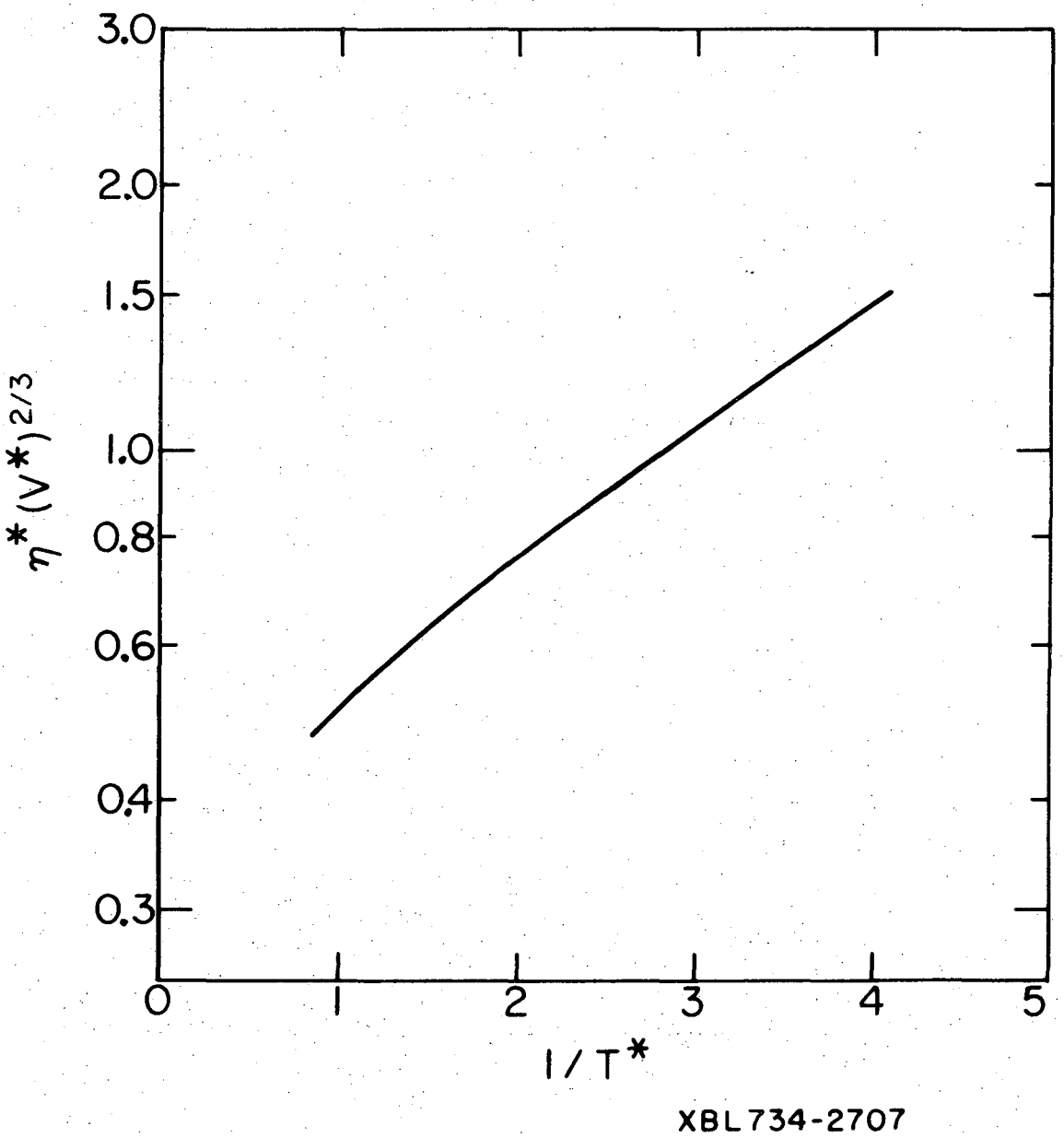

Fig. 17. Universal viscosity-temperature function for the alkali metals.

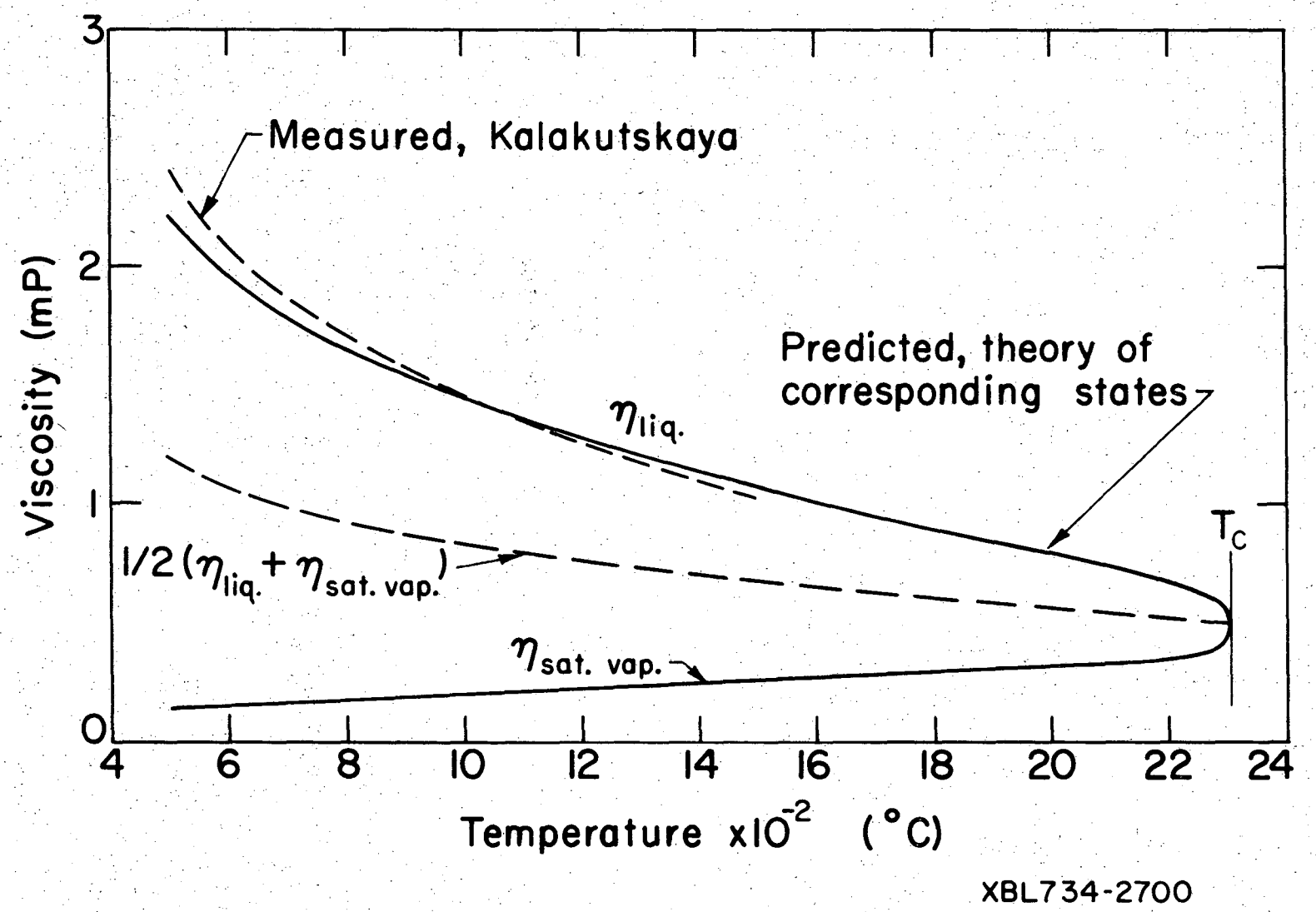

Fig. 18. Sodium viscosity calculated from the theory of corresponding states.

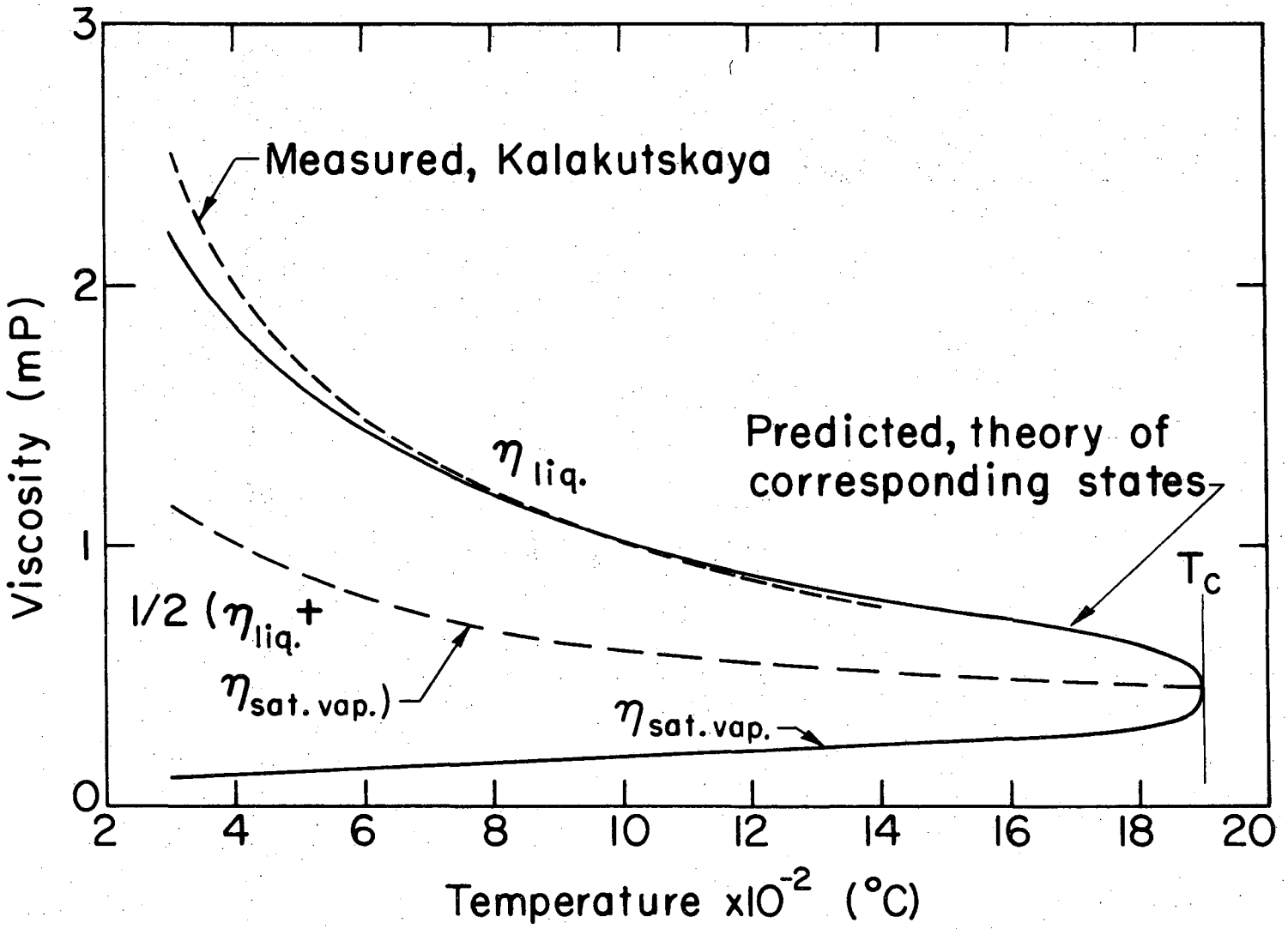

XBL734-2699

Fig. 19. Potassium viscosity calculated from the theory of corresponding states.

ACKNOWLEDGEMENTS

This work has been supported by the United States Atomic Energy Commission through the Lawrence Berkeley Laboratory.

I would like to thank Professor Donald R. Olander of the Department of Nuclear Engineering of the University of California for providing the stimulating topic as well as the noncoercive guidance and direct assistance which led to this thesis.

REFERENCES

1. Kirk-Othmer Encyclopedia of Chemical Technology, (John Wiley and Sons, New York, 1970), 2nd ed., Vol. 21, pp. 460-483.
2. C. V. Weaver and T. F. Stratton, Viscosity of Cesium Vapor, LA-DC-6135, Los Alamos Scientific Laboratory (1964).
3. D. I. Lee and C. F. Bonilla, The Viscosity of the Alkali Metal Vapors, Nucl. Eng. Des. 7, 455 (1968).
4. R. H. Stokes and R. Mills, Viscosity of Electrolytes and Related Properties, (Pergamon Press, Oxford, 1965), pp. 10-21.
5. D. E. Novak, Thorium Oxide Slurry Falling Ball Viscometer, CF-57-4-97, Oak Ridge National Laboratory (1957).
6. J. Rait, The Viscosity of Slags and Glasses, Trans. Brit. Cer. Soc., 40, 157 (1941).
7. R. Roscoe, Viscosity Determination by the Oscillating Vessel Method, Proc. Phys. Soc. 72, 576 (1958).
8. H. R. Thresh, Theory and Experiment in Methods for the Precision Measurement of Viscosity, Trans. ASM 55, 790 (1962).
9. S. Glasstone, K. J. Laidler and H. Eyring, Theory of Rate Processes, (McGraw-Hill, New York, 1941), pp. 477-500.
10. F. Reif, Fundamentals of Statistical and Thermal Physics, (McGraw-Hill, New York, 1965), pp. 471-478.
11. A. V. Grosse, Viscosities of Liquid Sodium and Potassium from Their Melting Points to Their Critical Points, Science 147, 1438 (1965).

12. R. G. Ross and D. A. Greenwood, Liquid Metals and Vapours Under Pressure, (Pergamon Press, Oxford, 1970), pp. 206-207.

13. J. A. De Mastery and N. M. Griesenauer, Elevated Temperature Corrosion Studies of Refractory Metal Alloys In Cesium Vapor and Lithium, Met. Soc. Conf. Vol. 41, (1965), p. 1169.

14. I. G. Dillon, P. A. Nelson and B. S. Swanson, Measurements of Densities and Estimation of Critical Properties of the Alkali Metals, J. Ch. Phys. 44, 4229 (1966).

15. H. Renkert and E. U. Franck, Electric Conductance of Cesium up to 2000°C and 1000 bars, (Ph.D. Thesis), Karlsruhe University, Germany (1969).

16. C. F. Bonilla, High Temperature Thermal Properties of Gases and Vapors, CU-2660-39, Columbia University, New York (1967).

17. J. P. Stone, C. T. Ewring, J. R. Spann, E. W. Steinkuller, D. D. Williams and R. R. Miller, J. Chem. Eng. Data 11, 315 (1966).

18. R. G. Ross and D. A. Greenwood, Liquid Metals and Vapours Under Pressure (Pergamon Press, Oxford, 1970), pp. 188-191.

19. T. W. Chapman, The Viscosity of Liquid Metals, A.I.Ch.E.J. 12, 395 (1966).

20. A. D. Pasternak, Liquid Metal Transport Properties, Phys. Ch. Liq. 3, 41 (1972).

21. M. R. Hopkins and T. C. Toye, The Determination of the Viscosity of Molten Metals, Proc. Phys. Soc. B63, 773 (1950).

22. J. S. Finucane and D. R. Olander, The Viscosity of Uranium and Two Uranium-Chromium Alloys, High Temp. Sci. 1, 466 (1969).

23. D. H. Niblett and J. Wilks, Dislocation Damping In Metals, Adv. Phys. 9, 1 (1960).

24. C. J. Smithells, Metals Reference Book, 4th ed., Vol. 3, (Plenum Press, New York, 1967), pp. 711-719.

25. R. P. Nelson, J. J. Rasmussen and O. D. Slagle, Properties of Molten Fast-Reactor Oxide Fuels, BNWL-1223, p. 2.21, Pacific Northwest Laboratory (1969).

26. T. E. Tietz and J. W. Wilson, Behavior and Properties of Refractory Metals, (Stanford University Press, Stanford, 1965), pp. 274-284.

27. H. C. Tsai and D. R. Olander, The Viscosity of Molten Uranium Dioxide, J. Nucl. Matl., 44, 83 (1972).

28. C. S. Lee, D. I. Lee and C. F. Bonilla, Calculation of the Thermodynamic and Transport Properties of Sodium, Potassium, Rubidium and Cesium Vapors to 3000°K, Nucl. Eng. Des. 10, 83 (1969).

29. P. Y. Achener and M. R. Boyer, Viscosity of Liquid Cesium and Rubidium, AGN-8192, Vol. 3, Aerojet-General Nucleonics (1966).

30. Cailletet and Mathias, Research on the Density of Liquified Gases and Their Saturated Vapors, Compt. Rend. 102, 1202 (1886).

31. E. N. Da C. Andrade, A Theory of the Viscosity of Liquids, Phil. Mag. J. Sci. 17, 698 (1934).

32. F. Reif, Fundamentals of Statistical and Thermal Physics, (McGraw-Hill, New York, 1965), pp. 173-174.

33. E. Helfand and S. Rice, Principle of Corresponding States for Transport Properties, J. C. Phys. 32, 1642 (1960).

34. N. A. Kalakutskaya, Viscosity of Liquid Alkali Metals Potassium, Sodium and Lithium at High Temperatures up to 1500°C, High Temp. 6, 436 (1968).

LEGAL NOTICE

This report was prepared as an account of work sponsored by the United States Government. Neither the United States nor the United States Atomic Energy Commission, nor any of their employees, nor any of their contractors, subcontractors, or their employees, makes any warranty, express or implied, or assumes any legal liability or responsibility for the accuracy, completeness or usefulness of any information, apparatus, product or process disclosed, or represents that its use would not infringe privately owned rights.

TECHNICAL INFORMATION DIVISION
LAWRENCE BERKELEY LABORATORY
UNIVERSITY OF CALIFORNIA
BERKELEY, CALIFORNIA 94720